

Old Dominion University

## ODU Digital Commons

---

Civil & Environmental Engineering Theses &  
Dissertations

Civil & Environmental Engineering

---

Spring 2-1-1971

### Static and Dynamic Buckling of Shallow Arches

David D. Loendorf  
*Old Dominion University*

Follow this and additional works at: [https://digitalcommons.odu.edu/cee\\_etds](https://digitalcommons.odu.edu/cee_etds)



Part of the [Civil Engineering Commons](#), and the [Structural Engineering Commons](#)

---

#### Recommended Citation

Loendorf, David D.. "Static and Dynamic Buckling of Shallow Arches" (1971). Master of Science (MS), Thesis, Civil & Environmental Engineering, Old Dominion University, DOI: 10.25777/e1c4-h957  
[https://digitalcommons.odu.edu/cee\\_etds/126](https://digitalcommons.odu.edu/cee_etds/126)

This Thesis is brought to you for free and open access by the Civil & Environmental Engineering at ODU Digital Commons. It has been accepted for inclusion in Civil & Environmental Engineering Theses & Dissertations by an authorized administrator of ODU Digital Commons. For more information, please contact [digitalcommons@odu.edu](mailto:digitalcommons@odu.edu).

122

STATIC AND DYNAMIC BUCKLING OF SHALLOW ARCHES

By

David D. Loendorf

A Thesis submitted to the Faculty of

OLD DOMINION UNIVERSITY

in partial fulfillment of the

requirements for the degree of

Master of Engineering

in

Civil Engineering

APPROVED:

---

Chairman, Dr. F. W. Barton  
Associate Professor of Engineering, UVA  
Formerly Adjunct Professor of Engineering, ODU

February 1971

## ABSTRACT

The static and dynamic buckling behaviors of a shallow, simply supported sinusoidal arch subjected to both a uniformly distributed step pressure load and a purely impulsive load are considered. Five equilibrium paths are obtained for the arch under static loading conditions. Critical static loads corresponding to two different instability modes and based on characteristics in the load displacement curve are obtained numerically. Critical dynamic loads, corresponding to three different instability modes, are obtained from a numerical procedure in which buckling criteria are based on characteristics in the time response of the structure. The influence of damping on the various dynamic stability regions and the dynamic response of a pre-loaded arch are observed and discussed.

TABLE OF CONTENTS

|  | Page |
|--|------|
| ABSTRACT . . . . .                             | ii   |
| ACKNOWLEDGMENTS . . . . .                      | v    |
| LIST OF TABLES . . . . .                       | vi   |
| LIST OF FIGURES . . . . .                      | vii  |
| NOTATION . . . . .                             | viii |
| 1. INTRODUCTION                                |      |
| 1.1 Statement of Problem . . . . .             | 1    |
| 1.2 Background History . . . . .               | 2    |
| 1.3 Object and Scope . . . . .                 | 4    |
| 2. EQUATIONS                                   |      |
| 2.1 Derivation of Governing Equation . . . . . | 6    |
| 2.2 Nondimensionalization . . . . .            | 8    |
| 2.3 Finite Difference Representation . . . . . | 9    |
| 2.4 Loading Conditions . . . . .               | 10   |
| 2.5 Initial Geometry . . . . .                 | 11   |
| 2.6 Boundary Condition . . . . .               | 12   |
| 3. NUMERICAL PROCEDURE                         |      |
| 3.1 Static Case . . . . .                      | 13   |
| 3.2 Dynamic Case . . . . .                     | 17   |
| 3.3 Prestress . . . . .                        | 19   |
| 4. STABILITY CRITERIA                          |      |
| 4.1 General . . . . .                          | 21   |
| 4.2 Static Symmetric . . . . .                 | 21   |
| 4.3 Static Asymmetric . . . . .                | 21   |
| 4.4 Dynamic Symmetric . . . . .                | 22   |
| 4.5 Dynamic Delayed Snapping . . . . .         | 22   |
| 4.6 Dynamic Asymmetric . . . . .               | 23   |

|                            | Page |
|----------------------------|------|
| 5. RESULTS AND DISCUSSION  |      |
| 5.1 General . . . . .      | 25   |
| 5.2 Static Case . . . . .  | 25   |
| 5.3 Dynamic Case . . . . . | 27   |
| SUMMARY . . . . .          | 30   |
| REFERENCES . . . . .       | 32   |
| TABLES . . . . .           | 34   |
| APPENDIX 1 . . . . .       | 36   |
| APPENDIX 2 . . . . .       | 38   |
| FIGURES . . . . .          | 52   |

## ACKNOWLEDGMENTS

The author extends his appreciation to Dr. Furman W. Barton for his continual supervision, advice, and suggestions as adviser of this thesis. Thanks are also due NASA Langley Research Center for their support of this study through Research Grant NGL 47-005-098.

David D. Loendorf

LIST OF TABLES

| Table                               | Page |
|-------------------------------------|------|
| 1. Critical Static Loads . . . . .  | 34   |
| 2. Critical Dynamic Loads . . . . . | 35   |

LIST OF FIGURES

| Figure   | Page |
|--|------|
| 1. Shallow arch . . . . .  | 52   |
| 2. Differential element . . . . .  | 53   |
| 3. Static load deflection curve . . . . .                                    | 54   |
| 4. Asymmetric static load deflection curve . . . . .                         | 55   |
| 5. Symmetric response . . . . .  | 56   |
| 6. Symmetric buckling criteria . . . . .                                     | 57   |
| 7. Arch configurations during symmetric snap-through . . . . .               | 58   |
| 8. Typical dynamic response . . . . .  | 59   |
| 9. Arch configurations during delayed snapping . . . . .                     | 60   |
| 10. Asymmetric buckling criteria . . . . .                                   | 61   |
| 11. Static stability curve . . . . .   | 62   |
| 12. Dynamic step buckling loads . . . . .                                    | 63   |
| 13. Dynamic impulsive buckling loads . . . . .                               | 64   |
| 14. Asymmetric step buckling loads with damping . . . . .                    | 65   |
| 15. Step buckling loads for delayed snapping with damping . . . . .          | 66   |
| 16. Effect of static prestress on critical step<br>symmetric loads . . . . . | 67   |

## NOTATION

|        |   |
|--------|---|
| A      | area of arch cross section  |
| {a}    | vector of correction factors in Newton-Raphson technique; see equation (29) |
| C      | damping parameter; see equation (1)   |
| $C_c$  | critical damping parameter = $2m\omega_0$                                   |
| E      | Young's modulus   |
| e      | nondimensional arch rise = $H/k$  |
| F      | force in impulse integral; see equation (16)                                |
| {f}    | vector of constants in Newton-Raphson technique; see equation (26)          |
| H      | arch rise; see figure 1   |
| h      | time interval   |
| $H(t)$ | heaviside step function   |
| I      | moment of inertia of arch cross section                                     |
| i      | finite difference station   |
| j      | iteration step number   |
| k      | radius of gyration of arch cross section                                    |
| L      | span of arch  |
| M      | moment acting on differential element                                       |
| m      | mass per unit length  |
| N      | number of interior difference stations                                      |
| n      | arch mode number; see equation (31)   |
| $N_x$  | axial force   |

|                    |   |
|--------------------|---|
| $\bar{N}_x$        | nondimensional axial force = $N_x L^2 / \pi^2 EI$       |
| $p(x,t)$           | time-dependent applied loading                          |
| $q(x,t)$           | nondimensional applied loading = $p(x,t)L^4 / \pi^4 EI$ |
| $q_{max}$          | amplitude of sine load                                  |
| $q_0$              | amplitude of nondimensional distributed load            |
| $t$                | time  |
| $V$                | shear acting on differential element                    |
| $v$                | velocity; see equation (30)                             |
| $w$                | arch displacement; see figure 1                         |
| $w_0$              | initial displacement; see figure 1                      |
| $\bar{w}$          | nondimensional arch displacement = $w/k$                |
| $\bar{w}_0$        | nondimensional initial displacement = $w_0/k$           |
| $\bar{w}_a$        | antisymmetric response component                        |
| $\bar{w}_s$        | symmetric response component                            |
| $x$                | coordinate along arch span                              |
| $\alpha$           | nondimensional damping parameter = $2\lambda$           |
| $\beta$            | Newmark's constant; see equation (30)                   |
| $\Delta$           | finite difference space                                 |
| $\delta(t - \eta)$ | delta function  |
| $\epsilon$         | duration of impulsive load                              |
| $\Lambda$          | axial displacement                                      |
| $\lambda$          | nondimensional damping coefficient = $c/2m\omega_0$     |

$\xi$

nondimensional coordinate along arch axis =  $\pi x/L$

$\tau$

nondimensional time =  $\omega_0 t$

$T$

nondimensional frequency =  $2\pi/n^2$

$\omega_0$

frequency

## 1. INTRODUCTION

### 1.1 Statement of Problem

When a shallow curved structure, such as an arch or curved panel, is subjected to a sufficiently large static load, buckling may occur. Similarly, if the structure is loaded dynamically, a buckling condition may also be achieved. In the dynamic case, however, the total response of the arch must be considered and the time dependency of the response, in addition to the spatial dependency of the static case, considerably complicates the analysis.

During recent years, much research has been conducted in the area of shallow curved structures because of the aerospace industry's need for a structure of minimum weight and maximum strength capable of carrying substantial loads. Because such structures may be loaded both statically and dynamically, a knowledge of their stability behavior under such loadings is of great importance.

A broad definition of the term stability was presented in reference [13] and is included here because it represents the basic idea from which both the static and dynamic instability criteria will be developed in this study.

A structure is in a stable state if admissible finite disturbances of its initial static or dynamic equilibrium are followed by displacements whose magnitude remains within allowable bounds during the lifetime of the structure.

The allowable displacements depend entirely on the intended use of the structure. Therefore, snap-buckling which might be defined as a

complete reversal of curvature for some finite increase in loading would be one area of interest both statically and dynamically. Equally important, however, might be the case in which snap-buckling does not occur, yet the dynamic growth in some response component becomes large enough to render the structure useless. Classical or bifurcation buckling may occur in both the static and dynamic case but, in general, is not the controlling form of instability for shallow structures.

### 1.2 Background History

Past research of the buckling phenomena has been accomplished in two different areas. The first, a static analysis, was observed by Fung and Kaplan [1] in 1952. A closed-form solution for the critical buckling load as defined by classical theory was obtained for shallow sinusoidal arches under different loading conditions by approximating the load, initial shape, and deflected shape in terms of Fourier series. For small arch rises the buckling mode was found to be symmetric, and for larger arch rises it was asymmetric. If a uniform load was used instead of a sinusoidal one, the critical uniform load was  $\pi/4$  times the critical sinusoidal one. Fung and Kaplan also looked at the effect of initial shape and found that it had little effect on the buckling load provided it was symmetric. Also that year, Hoff and Bruce [2] looked at this same static problem, with similar results, and also approached the second area of interest, that of dynamic response analysis. With the use of energy contours, a closed-form solution was derived for critical buckling loads of shallow arches under the presence of both step loadings of infinite duration and impulsive loadings.

Since that time most research has been directed toward the dynamic analysis trying to define what is dynamic buckling or will a suddenly applied load, which is less than the critical static load, cause buckling. Humphreys [3] in 1966 investigates snap-buckling of shallow arches by solving the nonlinear equations of motion numerically, using the first six modes and an approximate Galerkin technique. Results were presented for step and impulsive dynamic loadings. Lock [4,5] investigated dynamic buckling for both sinusoidal uniform loadings and pulse loadings, using an analysis in which the arch displacement was represented by a finite series of normal modes (two-mode analysis). Lock also began to look at two different instabilities associated with dynamic response, those of symmetric and asymmetric, along with the effect of damping on the dynamic analysis. Fulton and Barton [6], in a paper presented in 1967, used a finite difference approximation of the governing equations which gave them an N-mode solution, where N was the number of interior difference stations. The equations of motion were solved numerically and both symmetric and asymmetric dynamic instabilities studied, including the suggestion for a new asymmetric buckling criterion. McCullers [7], in 1967, did an analysis of both static and dynamic buckling using a numerical approach, but was not able to correlate the deflected shapes of the static analysis to actual buckled shapes. Hsu [16,17] looked at dynamic stability of shallow sinusoidal arches for both impulsive loadings and timewise step loadings and presented a sufficiency criterion of dynamic stability against snap-through. Schreyer and Masur [12] used an energy approach to study static buckling

of clamped shallow circular arches under uniform loadings and obtained results similar to [1]. Other work in the area of stability of shallow arches has been accomplished by Hegemier and Teung [18], Cheung and Bubcock [8], Smitses [10], Cheung [9], and Vahidi [11].

As may be observed, there has been considerable research accomplished in the area of snap-buckling of shallow structures, both static and dynamic, but there does not seem to be any established criteria for defining the other instabilities associated with these structures. There is not even a consistent definition of dynamic buckling available. Those papers that approached the problem using a Fourier series or an energy approach have limitations in two areas. One is the number of modes possible in the solution, and second is the need for a new analysis whenever a parameter is to be changed. The energy approach also requires a static solution for use in obtaining dynamic results, and there is no consistent method of solution for both static and dynamic buckling.

### 1.3 Object and Scope

The equations of motion of the shallow arch are not as complicated or hard to work with as those of, say, a curved panel or shell. Therefore, the shallow arch, which possesses similar nonlinear response characteristics of the more complicated curved structures, will be adopted as the representative shallow curved structure used in this study.

The object of this study is to investigate the stability of shallow arches subjected to various static and dynamic loadings. To facilitate the study, primary emphasis will be placed on numerical

solutions of the governing differential equation to help develop and evaluate numerical procedures necessary to obtain criteria for identifying instabilities associated with both static and dynamic buckling. This also allows an essentially N-mode solution, where N is the number of nodes used to represent the structure in the finite difference approximation of the governing equation. Critical static buckling loads, along with those instabilities associated with dynamic response, will be studied for the general arch. Results obtained will be compared with those obtained by previous investigators. Also, the effect of various parameters on static and dynamic buckling will be studied. The initial shape of the arch will be sinusoidal for all cases studied because, according to Fung and Kaplan [1], the initial shape has very little effect on buckling characteristics provided it is shallow. Varying arch rises will be observed for the case of pinned-pinned supports. The loading conditions will be those of a uniform load of infinite duration for both the static and dynamic cases, and a purely impulsive load for the dynamic case. The dynamic response will be observed with viscous damping present and also under the influence of a preload.

## 2. EQUATIONS

### 2.1 Derivation of Governing Equation

Consider a shallow arch (fig. 1) of span  $L$  and rise  $H$  subjected to some time-dependent loading. Two methods are available for obtaining the governing differential equation of motion: An equilibrium method which sums forces and moments acting on a representative element of length  $dx$ , or an energy method which equates the first variation of the total potential energy of the element  $dx$  to zero. The equilibrium method is used in this analysis.

Referring to figure 2 and summing moments, the following equation is obtained:

$$\begin{aligned} M + p(x,t)(dx)\left(\frac{dx}{2}\right) + \left(V + \frac{\partial V}{\partial x} dx\right)dx - M - \frac{\partial M}{\partial x} dx \\ + m \frac{\partial^2 w}{\partial t^2}(dx)\left(\frac{dx}{2}\right) + c \frac{\partial w}{\partial t}(dx)\left(\frac{dx}{2}\right) = 0 \end{aligned} \quad (1)$$

Assuming higher degree terms are approximately zero, the above equation reduces to

$$V = \frac{\partial M}{\partial x} \quad (2)$$

Summing the vertical forces, including inertia and damping terms, the following equation is obtained.

$$\begin{aligned}
 & -V - N_x \left( \frac{\partial w_0}{\partial x} + \frac{\partial w}{\partial x} \right) + p(x,t) dx - \frac{m \partial^2 w}{\partial t^2} - C \frac{\partial w}{\partial t} + V + \frac{\partial V}{\partial x} dx \\
 & + N_x \left[ \left( \frac{\partial w_0}{\partial x} + \frac{\partial w}{\partial x} \right) + \left( \frac{\partial^2 w_0}{\partial x^2} + \frac{\partial^2 w}{\partial x^2} \right) dx \right] = 0 \quad (3)
 \end{aligned}$$

Again equating higher degree terms to zero reduces equation (3) to

$$p(x,t) dx - m \frac{\partial^2 w}{\partial t^2} dx - C \frac{\partial w}{\partial t} dx + \frac{\partial V}{\partial x} dx + N_x \left( \frac{\partial^2 w_0}{\partial x^2} + \frac{\partial^2 w}{\partial x^2} \right) dx = 0 \quad (4)$$

From equation (2),

$$\frac{\partial V}{\partial x} = \frac{\partial^2 M}{\partial x^2} = -EI \frac{\partial^4 w}{\partial x^4} \quad (5)$$

Equation (6) results from substituting equation (5) into equation (4), and is the nonlinear differential equation of motion used in this study.

$$-EI \frac{\partial^4 w}{\partial x^4} + N_x \left[ \frac{\partial^2 w_0}{\partial x^2} + \frac{\partial^2 w}{\partial x^2} \right] + p(x,t) - C \frac{\partial w}{\partial t} = m \frac{\partial^2 w}{\partial t^2} \quad (6)$$

$N_x$  is the axial thrust of the arch obtained from the relationship between the displacement and axial force

$$\Delta = \frac{N_x L}{AE} \quad (7)$$

or rearranging

$$N_x = \frac{AEA}{L} \quad (8)$$

where  $\Lambda$  is the axial shortening of the arch as it deflects and is equal to

$$\Lambda = \frac{1}{2} \int_0^L \left[ 2 \frac{\partial w}{\partial x} \frac{\partial w_0}{\partial x} + \left( \frac{\partial w}{\partial x} \right)^2 \right] dx \quad (9)$$

Substituting equation (9) into equation (8), the following equation is obtained for  $N_x$ .

$$N_x = \frac{EA}{2L} \int_0^L \left[ 2 \frac{\partial w}{\partial x} \frac{\partial w_0}{\partial x} + \left( \frac{\partial w}{\partial x} \right)^2 \right] dx \quad (10)$$

In equations (6) and (10),  $w_0$  is the initial shape,  $w$  is the displacement measured from  $w_0$ ,  $E$  is Young's modulus,  $I$  the moment of inertia,  $p(x,t)$  the time-dependent applied loading,  $C$  the damping coefficient,  $m$  the mass,  $A$  the cross-sectional area, and  $L$  the span of the arch.

## 2.2 Nondimensionalization

Introduce the following nondimensional variables:

$$\xi = \frac{\pi x}{L}, \quad \tau = \omega_0 t, \quad \lambda = \frac{C}{2m\omega_0}, \quad w = \bar{w}k$$

where

$$\omega_0 = \left( \frac{\pi}{L} \right)^2 \left( \frac{EI}{m} \right)^{1/2}, \quad k = \text{radius of gyration}$$

Equations (6) and (10) then take the form

$$-\frac{\partial^4 \bar{w}}{\partial \xi^4} + \bar{N}_x \left[ \frac{\partial^2 \bar{w}_0}{\partial \xi^2} + \frac{\partial^2 \bar{w}}{\partial \xi^2} \right] - \alpha \frac{\partial \bar{w}}{\partial \tau} + q(\xi, \tau) = \frac{\partial^2 \bar{w}}{\partial \tau^2} \quad (11)$$

$$\bar{N}_x = \frac{1}{2\pi} \int_0^\pi \left[ 2 \frac{\partial \bar{w}_0}{\partial \xi} \frac{\partial \bar{w}}{\partial \xi} + \left( \frac{\partial \bar{w}}{\partial \xi} \right)^2 \right] d\xi \quad (12)$$

where

$$q(\xi, \tau) = p(x, t) \frac{L^4}{\pi^4 EI k}$$

$$\bar{N}_x = \frac{N_x L^2}{\pi^2 EI}$$

and

$$\alpha = 2\lambda$$

### 2.3 Finite Difference Representation

The central finite difference approximations used in this study are

$$\begin{aligned} \left. \frac{\partial \bar{w}}{\partial \xi} \right|_i &= \frac{1}{2\Delta} \left[ \bar{w}_{i+1} - \bar{w}_{i-1} \right] \\ \left. \frac{\partial^2 \bar{w}}{\partial \xi^2} \right|_i &= \frac{1}{\Delta^2} \left[ \bar{w}_{i-1} - 2\bar{w}_i + \bar{w}_{i+1} \right] \\ \left. \frac{\partial^4 \bar{w}}{\partial \xi^4} \right|_i &= \frac{1}{\Delta^4} \left[ \bar{w}_{i-2} - 4\bar{w}_{i-1} + 6\bar{w}_i - 4\bar{w}_{i+1} + \bar{w}_{i+2} \right] \end{aligned} \quad (13)$$

where  $i$  is the  $i$ th finite difference station and  $\Delta$  the station spacing. If the spatial derivatives of equations (11) and (12) are replaced by the appropriate finite difference approximations, equation (11) is reduced to a set of coupled, nonlinear, ordinary differential equations in time of the form

$$\frac{d^2 \bar{w}_i}{d\tau^2} + \alpha \frac{d\bar{w}_i}{d\tau} + f(\bar{w}_0, \bar{w}_{i-2}, \dots, \bar{w}_{i+2}, \Delta, N_x) = q_0 \quad (14)$$

$$(i = 1, 2, \dots, N)$$

and equation (12) becomes

$$N_x = \frac{1}{2\pi} \int_0^\pi g(\bar{w}_0, \bar{w}_{i-1}, \bar{w}_{i+1}, \Delta) d\xi \quad (i = 1, 2, \dots, N) \quad (15)$$

where  $N$  equals the number of interior finite difference stations and  $\Delta$  the spacing.

#### 2.4 Loading Conditions

The primary loading conditions are those of a uniform step pressure of infinite duration and a uniform impulsive load. The uniform step pressure of infinite duration is defined as

$$q(\xi, \tau) = q_0 H(\tau) \quad (16)$$

where  $H(\tau)$  is the heaviside step function and  $q_0$  the magnitude of the load. The impulsive load is defined as

$$\text{Impulse} = \int_t^{t+\epsilon} F dt \quad (17)$$

Introducing the delta function  $\delta(t - \eta)$  which has the following properties

$$\begin{aligned} \delta(t - \eta) &= 0 && \text{for all } t \neq \eta \\ \int_0^{\infty} \delta(t - \eta) dt &= 1 && 0 < \eta < \infty \\ \int_0^{\infty} f(t) \delta(t - \eta) dt &= f(\eta) && 0 < \eta < \infty \end{aligned} \quad (18)$$

and the fact that  $F dt = M dv$ , it can be seen that at time  $t = \eta$  the impulse acting on the arch will result in a sudden change in the velocity with essentially zero displacement. Therefore, impulsive loadings have the following initial conditions:

$$\bar{w}_i = 0; \quad \frac{\partial \bar{w}_i}{\partial \tau} = \frac{\int F d\tau}{k^2 \omega_m} \quad (19)$$

## 2.5 Initial Geometry

The initial shape of the arch will be sinusoidal

$$\bar{w} = e \sin \xi \quad (20)$$

where

$$e = \frac{H}{k} \quad (21)$$

## 2.6 Boundary Condition

The boundary condition corresponding to simple supports is

$$\bar{w}(0, \tau) = \frac{\partial^2 \bar{w}}{\partial \xi^2}(0, \tau) = 0$$

$$\bar{w}(\pi, \tau) = \frac{\partial^2 \bar{w}}{\partial \xi^2}(\pi, \tau) = 0$$
(22)

In finite difference notation the boundary condition for simple supports is

$$\bar{w}_2 = 0$$

$$\bar{w}_1 = -\bar{w}_3$$

$$\bar{w}_{n+1} = 0$$

$$\bar{w}_{n+2} = \bar{w}_n$$
(22a)

This will be the only boundary condition observed.

### 3. NUMERICAL PROCEDURE

#### 3.1 Static Case

By taking equation (11) and reducing it to the static case by disregarding the time-dependent terms and then expanding in terms of the finite difference approximations of equation (13), the following static equation of motion is obtained:

$$\begin{aligned} \bar{w}_{i-2} - (4 + \bar{N}_x \Delta^2) \bar{w}_{i-1} + (6 + 2\bar{N}_x \Delta^2) \bar{w}_i - (4 + \bar{N}_x \Delta^2) \bar{w}_{i+1} \\ + \bar{w}_{i+2} - \left( q_i + \bar{N}_x \bar{w}_o'' \right) \Delta^4 = 0 \end{aligned} \quad (23)$$

where primes denote differentiation with respect to  $\xi$  and  $\bar{N}_x$  is the nondimensional axial thrust which has the following form upon substitution of the finite difference approximations

$$\begin{aligned} \bar{N}_x = \frac{1}{2\pi} \int_0^\pi \frac{1}{2\Delta^2} \left[ (\bar{w}_{o_{i+1}} - \bar{w}_{o_{i-1}})(\bar{w}_{i+1} - \bar{w}_{i-1}) \right. \\ \left. + \frac{1}{2}(\bar{w}_{i+1} - \bar{w}_{i-1})^2 \right] d\xi \end{aligned} \quad (24)$$

Equations (23) and (24) are now left with only two variables,  $q_i$  and  $\bar{w}_i$ , and the response of the arch is determined by either of two methods. In the numerical procedure, integration with respect to the spatial variable in equation (24) is performed using Simpson's rule. Also, a direct iteration approach, such as assuming a load and calculating a deflection will not yield satisfactory load-deflection curves

because of the multiple roots associated with the governing equations under certain loading conditions. However, a method is developed in this study whereby all roots of the governing equations are determined.

The first method is limited to symmetric displacements by working with the left-hand side of the arch, setting the right-hand side displacements and loads equal to the corresponding ones on the left.

Portions of the load-deflection curve are obtained iteratively by assuming initial displacements at each node ( $\bar{w}_i$ ) and solving equations (23) and (24) for the nodal loads ( $q_i$ ). An average nodal load is then determined by summing all the nodal loads and dividing by the number of nodes. This average load is then compared with each nodal load ( $q_i$ ) and adjustments made to the corresponding nodal displacements ( $\bar{w}_i$ ) according to the following relationship:

$$\bar{w}_i = \bar{w}_i \pm \text{ABS} \left[ \frac{q_i}{q_{av}} \times \frac{\bar{w}_{i+1}}{\bar{w}_i} \times \text{factor} \right] \quad (25)$$

where the  $\pm$  sign would depend on whether the load needed to be increased or decreased, and factor is a constant that may be changed to help convergence. On the next iteration a new average load is determined and adjustments made to the displacements as above. This procedure continues until all nodal loads ( $q_i$ ) converge to the average load pertaining to that iteration. It is interesting to note that an initial load on which to converge is never specified, only an initial displacement. If a sinusoidal load is desired, then the average load is used as a  $q_{\max}$  from which the other  $q_i$  are determined and comparisons made as in the

above procedure. This method will be referred to hereafter as the "assumed displacement method."

The second method of analysis is not restricted to symmetric shapes and again uses equation (23) to form a set of coupled, nonlinear, algebraic equations in terms of the  $\bar{w}_i$ 's, which are solved using a Newton-Raphson technique as presented in reference [15], and discussed below. Assume

$$\begin{aligned} f_1 &= \text{eq. (23)} \Big|_{I=3} \\ f_2 &= \text{eq. (23)} \Big|_{I=4} \\ &\vdots \\ f_N &= \text{eq. (23)} \Big|_{I=N+2} \end{aligned} \quad (26)$$

Using the recurrence formulas of reference [15], the following are obtained

$$\begin{aligned} a_3 \frac{\partial f_{1j}}{\partial \bar{w}(3)} + a_4 \frac{\partial f_{1j}}{\partial \bar{w}(4)} + \dots + a_{N+2} \frac{\partial f_{1j}}{\partial \bar{w}(N+2)} &= -f_{1j} \\ a_3 \frac{\partial f_{2j}}{\partial \bar{w}(3)} + \dots &\vdots \\ &\vdots \\ &\vdots \\ a_3 \frac{\partial f_{Nj}}{\partial \bar{w}(3)} + \dots + a_{N+2} \frac{\partial f_{Nj}}{\partial \bar{w}(N+2)} &= -f_{Nj} \end{aligned} \quad (27)$$

where  $\{a_i\}$  is the vector of correction factors

$$a_i = \bar{w}(i)_{j+1} - \bar{w}(i)_j \quad (j = 1, 2, \dots) \quad (28)$$

and  $i$  equals the  $i$ th difference station and  $j$  equals the  $j$ th iteration.

In matrix notation, equations (27) are

$$\begin{bmatrix} \frac{\partial f_1}{\partial \bar{w}(3)} & \frac{\partial f_1}{\partial \bar{w}(4)} & \dots & \frac{\partial f_1}{\partial \bar{w}(N+2)} \\ \frac{\partial f_2}{\partial \bar{w}(3)} & & & \\ \vdots & & & \\ \frac{\partial f_N}{\partial \bar{w}(3)} & \dots & \dots & \frac{\partial f_N}{\partial \bar{w}(N+2)} \end{bmatrix} \begin{bmatrix} a_3 \\ a_4 \\ \vdots \\ a_{N+2} \end{bmatrix} = \begin{bmatrix} -f_1 \\ -f_2 \\ \vdots \\ -f_N \end{bmatrix} \quad (29)$$

By assuming an initial load  $q_i$  and a deflected shape  $\bar{w}_i$ , equations (29) may be solved for the  $\{a\}$  vector simultaneously which gives the correction factors for the displacements  $\bar{w}_i$ .

In the previous method, convergence of nodal loads was required. In this method, convergence of nodal displacements is required for a given loading. This method, which is not restricted to symmetric displacements, will be referred to as the "assumed load method." Appendix 2 contains a Fortran program of this method.

### 3.2 Dynamic Case

It is assumed that at some time  $\tau_n$  the acceleration, velocity, and displacements of the finite difference stations represented in equation (13) are known, but nothing is known about the stations at time  $\tau_{n+1}$ . By the use of Newmark's beta method, presented in reference [14] and discussed here, an acceleration at time  $\tau_{n+1}$  is assumed and velocities and displacements calculated from the following relationships:

$$v_{n+1} = v_n + \frac{h}{2}(a_n + a_{n+1})$$

$$w_{n+1} = w_n + v_n h + \left(\frac{1}{2} - \beta\right)h^2(a_n + \beta a_{n+1})$$
(30)

where  $h$  is the time interval and  $\beta$  a multivalued constant which describes the variation in acceleration during the time interval. For the purpose of this study,  $\beta$  will be chosen equal to  $1/6$  which corresponds to a linear variation of the acceleration during the time interval. Convergence and stability criteria are investigated by the author of reference [14] and it is determined that for a  $\beta = 1/6$  if the time interval is chosen for convergence, then the numerical procedure is always stable. To determine what the required time interval is, it will be necessary to look at the periods corresponding to the  $N$ -modes of the arch where  $N$  is the number of difference stations. The nondimensional frequency is defined as

$$\gamma = \frac{2\pi}{n^2} \quad (n = 1, 2, \dots, N)$$
(31)

where the fundamental frequency corresponds to an  $n = 1$ . It is quite obvious that if convergence is established for the highest possible mode, then convergence is established for all modes of the system. Therefore, since this study is being made with 13 difference stations and the fact that  $h/\tau \leq 0.389$  (ref. [14]), the time interval  $h$  used in this study will be 0.01, which satisfies all convergence criteria for all of the  $n$ -modes of the arch.

Consider now the numerical iterative procedure used. For a given load and an assumed initial value of the acceleration at the  $(n+1)$  time step, the velocity and displacements are calculated by use of equation (30). These values of velocity and displacement are then used in equation (14) to calculate an acceleration. A comparison is then made between the assumed and calculated accelerations. If it is within set tolerance limits, the process is complete for that time step; if the tolerance is not satisfied, then the calculated acceleration is used as the new assumed acceleration and the process repeated within that time step until convergence is attained. The time is then incremented and the above procedure repeated. At convergence, the acceleration, velocity, and displacements are known for that given loading condition and that particular point in time from which response plots may be made. The symmetric response component is defined in terms of an average displacement parameter

$$\bar{w}_s = \frac{\sum \bar{w}_i}{\sum (\bar{w}_0)_i} \quad (32)$$

and the antisymmetric response component,  $\bar{w}_a$ , is defined as the algebraic difference of the displacements at the quarter points normalized with respect to the corresponding  $\bar{w}_0$ . Normally, some asymmetry in the initial conditions is required to introduce antisymmetric components in the response. In this study, computer round-off errors are allowed to perform this function.

The nondimensional damping parameter in equation (11) is defined as

$$\alpha = 2\lambda = \frac{C}{m\omega_0} \quad (33)$$

$C_c$ , the critical damping factor, is defined as

$$C_c = 2m\omega_0 \quad (34)$$

therefore,  $\lambda$  is actually the damping ratio

$$\lambda = \frac{C}{C_c} \quad (35)$$

and for zero damping has a value of zero. For finite damping to be included in the numerical analysis,  $\lambda$  will have a value equal to some percentage of the critical damping and is accomplished by simply changing an input parameter.

### 3.3 Prestress

When a prestress analysis is desired, the static and dynamic cases are merged together in the following manner: Static displacements corresponding to prestress or preload conditions are determined from a static analysis as described in Section 3.1. A dynamic analysis is

then made as described in Section 3.2 using the displacements calculated in the static analysis as initial displacements rather than the previous condition of zero displacements initially.

#### 4. STABILITY CRITERIA

##### 4.1 General

Previous investigators have used the general criteria for symmetric buckling used in this study and discussed below. Limited use has been made of the other criteria, especially that for the dynamic asymmetric buckling. All criteria discussed below was confirmed by this study before being applied.

##### 4.2 Static Symmetric

Consider the static load deflection curve of figure 3. As the uniform load on the arch is increased, the displacement follows the almost linear portion of the curve from zero to A, provided the initial shape of the arch is symmetric. At point A, any finite increase in the load results in a large displacement to point C or, by definition, snap-buckling occurs. This is the criterion used to determine static symmetric buckling and the load corresponding to point A of figure 3 is called the critical static symmetric load.

##### 4.3 Static Asymmetric

The static symmetric criterion for buckling requires the arch to be initially symmetric. In actual structures this is rarely true and an analysis is necessary which includes initial imperfections in the arch geometry. Consider figure 4 which is a static load deflection curve if the initial shape is given some imperfection of the second mode. From zero to A, the arch may converge to either a symmetric shape (represented by the line OA) or an asymmetric shape (represented

by the line AB). For a load above point A, snap-through corresponding to point C is the only possible configuration with imperfections present in the initial geometry. Therefore, the load corresponding to point A is called the critical static antisymmetric buckling load.

#### 4.4 Dynamic Symmetric

If the displacement response of the arch is plotted as a function of time, as in figure 5, it is observed that for two different load levels there is a large discrepancy in peak response during the first period of oscillation. Figure 6 is a plot of these peak displacements as a function of loading and clearly shows a jump discontinuity or snap-through. This large variation in peak values of the symmetric response during the first period of oscillation is the criterion used to obtain the critical dynamic symmetric buckling load. If the response of the arch under the critical symmetric buckling load is output on a cathode ray tube display unit, the arch configurations in figure 7 are observed as the arch buckles. A complete set of buckling configurations is shown in Appendix 1. Note the symmetry of the arch during snap-through.

#### 4.5 Dynamic Delayed Snapping

Consider the response plots shown in figure 8 which are for a load less than the critical load required for dynamic symmetric snap-through. During the first few cycles of oscillation the symmetric component of response is harmonic with amplitude much less than the arch rise and the asymmetric component is essentially zero. However, after several cycles of oscillation, snap-through again occurs and is

due to the large and rapid growth in the asymmetric component. This type of buckling is due to the coupling between the symmetric and asymmetric components of response and referred to as dynamic delayed snapping. The criterion for obtaining dynamic delayed snapping loads is the same as that used for dynamic symmetric with the exception that it will occur sometime subsequent to the first period of oscillation. The arch response again observed using the cathode ray tube is quite different from the response of the symmetric case. The arch oscillates in a symmetric mode for a number of cycles, or until the asymmetric component begins to grow (fig. 8), at which time the arch response becomes asymmetric. Figure 9 shows various arch shapes as snap-through occurs, while Appendix 1 contains a complete set of configurations observed during buckling. The coupling of the modes is quite obvious when observed this way.

#### 4.6 Dynamic Asymmetric

For certain conditions of arch geometry and loading, the asymmetric component of response grows appreciably without any noticeable growth in the symmetric component. This seems to point to the fact that criteria based on the symmetric component are not sufficient to label the instabilities of the arch under dynamic loading and a criterion based on the asymmetric component of response is needed. Since in this study the loading is symmetric, computer round-off is used to initiate the growth in the asymmetric component. Consider figure 10 which shows the peak amplitude of the asymmetric component as a function of loading for nondimensional response times of 20, 50, and 200. For sufficiently

small loads, no growth occurs. Above some critical value, however, growth initiates immediately after load application and grows to some limiting value with time. The load at which growth in the asymmetric component is initiated is used as the criterion for defining the critical dynamic antisymmetric buckling load. This same criterion was suggested in an earlier study [6].

## 5. RESULTS AND DISCUSSION

### 5.1 General

Initial numerical computation was accomplished using an IBM 1130 computing system because its interaction capabilities were very useful during preliminary studies. However, due to the volume of data output and the long response times required for portions of the dynamic analysis, a high-speed CDC 6600 computing system was used to obtain final instability data.

### 5.2 Static Case

Consider the static stability curve of figure 11 for an arch rise of  $e = 8$ . The equilibrium points defining the five branches of the curve are determined by assuming an equilibrium configuration corresponding to a given applied load and converge to the correct shape using the Newton-Raphson procedure described earlier in the "assumed load method."

Specifically, the stable symmetric branch OAB is determined directly by assuming an initial shape that is symmetric and then using the last converged shape as the new assumed shape while incrementing the load. Point B, corresponding to a load of  $P = 31.9$ , is the critical symmetric buckling load as defined by criterion previously discussed. Once snap-buckling has occurred, the snapped equilibrium branch HGFE is determined as above by assuming the converged shape as the new assumed shape and then decrementing the load. At point F, the arch will snap back to the original upright position. The determination

of the unstable branches AG, CD, and BE requires a slight modification in the direct procedure. For branch AG, various amounts of the second mode, or first antisymmetric mode, are assumed in the initial shape and the Newton-Raphson procedure used to converge to the correct shape. At some point in the loading, the assumed initial asymmetry is such that convergence is to the unstable asymmetric branch AG. This asymmetric shape is then assumed as the new initial shape and the load incremented and/or decremented as required to complete the branch. Point A, corresponding to a load of  $P = 22.24$ , is the critical asymmetric buckling load as defined by criterion. Since branches AG and OA are nearly linear, their intersection point is easily determined numerically once two points on each branch are determined. This intersection point is defined as the critical asymmetric load. The unstable symmetric branches BE and CD are obtained in a manner similar to the asymmetric branch AG, only now the initial shape has various combinations of the first and third modes present. The critical symmetric loads and equilibrium points on branches OAB and BE are also determined using the "assumed displacement method." Results are identical to those obtained using the "assumed load method" and provide an excellent check on the numerical process.

Critical static buckling loads for various arch geometries, determined in the same manner as those for the arch rise of  $e = 8$ , are given in table 1 along with the critical loads as determined from reference [1]. The discrepancy in the critical symmetric loads is explained by again considering figure 11. The dotted portion of the

unstable symmetric branch CD is assumed, using the critical load determined from reference [1] which uses a single-term approximation for the deflected shape. In this study the deflected shape has 13 modes and, numerically, the arch buckles prior to reaching the dotted portion. The five equilibrium paths, two stable and three unstable, are also observed in reference [8].

### 5.3 Dynamic Case

Dynamic buckling loads, corresponding to three modes of dynamic instability, are plotted as a function of arch rise for uniform loads in figure 12 and for impulsive loads in figure 13. Also included in each figure is a curve representing the static buckling loads determined previously in this study.

Considering figures 12 and 13, the curves for symmetric buckling indicate the significantly larger loads required for snapping by a purely symmetric response. The effect of antisymmetric modes in the response is indicated by the decrease in critical loads for delayed snapping. The stability curves for asymmetric buckling differ markedly from the curves corresponding to snap-buckling.

Asymmetric buckling loads are consistently lower than the other and, in fact, tend toward zero in two places along the boundaries. However, these lower boundaries represent only the initiation of growth in the antisymmetric response and not snap-through. Nevertheless, asymmetric buckling should not be disregarded. Growth in the asymmetric response is sufficient for displacements to achieve a magnitude on the order of 20 percent of the arch rise along the lower boundaries of the

asymmetric buckling region and, just prior to delayed snapping, the magnitude of the asymmetric response is of the order of the arch rise.

The results show the somewhat similar buckling response observed for the uniformly distributed step load and the uniformly distributed impulse. The values of arch rise for which the asymmetric buckling resistance approaches zero are identical for the two loading conditions. However, asymmetric buckling for the uniform step load is only defined for values of  $e$  less than approximately 11, while asymmetric buckling associated with the uniform impulsive load was present for all values of arch rise. Figures 12 and 13 also show that for the larger values of arch rise, critical step loads for delayed snapping are only slightly less than the static snap-buckling loads, while critical impulsive loads required for delayed snapping are significantly less.

When damping is retained in the analysis the criteria for identifying the three modes of instability remain valid. As would be expected, the influence of damping has negligible effect on the critical symmetric buckling loads for both of the loading conditions studied. However, stability boundaries defined by delayed snapping and asymmetric buckling are modified appreciably by the effects of damping.

Critical uniform step loads for asymmetric buckling are plotted in figure 14 as a function of arch rise for damping ratios corresponding to zero and 1 percent of critical damping. As indicated, the critical loads are increased with the addition of damping and the asymmetric growth is correspondingly reduced, particularly in the two regions of low stability resistance. Numerical results indicate that

damping ratios above approximately 5 percent are sufficient to eliminate the asymmetric buckling mode entirely. The presence of damping also serves to appreciably increase critical uniform step loads for delayed snapping as indicated in figure 15. For an arch rise greater than approximately  $e = 9$ , the critical uniform step load for delayed snapping is the same as the static buckling load for any finite value of damping. A similar observation was reported in [18].

For an arch subjected to a uniform impulse load, the presence of damping had noticeable effect only on the critical loads for delayed snapping; in fact, the delayed snapping form of dynamic buckling is completely eliminated with damping present. Critical impulsive loads for asymmetric buckling are increased slightly for finite amounts of damping.

The effect of initial static prestress on critical symmetric loads is shown in figure 16. As expected, for a prestress load of zero the critical symmetric load is that given in table 2, and for a prestress load equal to the critical static load the critical symmetric load is zero. For all values of prestress between these two extremes, the critical symmetric load is linearly related to the level of prestress. A similar result is observed in reference [7].

## SUMMARY

The static and dynamic buckling behavior of a shallow sinusoidal arch with pinned ends is studied. The loadings considered consist of a uniformly distributed step load of infinite duration and a purely impulsive load. The effects of finite damping and static prestress are also observed.

A method is devised whereby static equilibrium branches of the load displacement curve are determined numerically using the same discrete model adopted for the dynamic analysis. Specifically, the static differential equation is reduced to a set of nonlinear algebraic equations using finite difference approximations and then solved using a Newton-Raphson procedure. Critical static loads for symmetric and asymmetric buckling are determined from criteria based on characteristics in the equilibrium branches.

The dynamic analysis consists of a direct numerical integration of the nonlinear equations of motion obtained from a finite difference approximation. Critical symmetric, asymmetric, and delayed snapping loads, for both loading conditions, are determined from criteria based on characteristics in the time response of the arch. Results indicate somewhat similar buckling response for both loading conditions. However, critical impulsive loads are always less than corresponding critical step loads. Regions of extremely low asymmetric step buckling loads correspond identically to regions of extremely low asymmetric impulse buckling loads.

The influence of damping on critical loads is studied for both step and impulsive loads. Sufficient damping markedly reduces those regions of asymmetric step buckling where the critical load approaches zero but has little effect on those regions defined for asymmetric impulsive buckling. For finite values of damping, the critical step load for delayed snapping is the same as the static snapping load for sufficiently large arch rises. For the impulse loading, damping completely eliminates delayed snapping, and the only two instability mechanisms present are the symmetric and asymmetric.

Results for a structure with prescribed prestress subjected to a suddenly applied dynamic load indicate a linear relationship between the critical dynamic load and the level of prestress.

#### REFERENCES

1. Fung, Y. C.; and Kaplan, A.: "Buckling of Low Arches or Curved Beams of Small Curvature," NACA TN 2840, Nov. 1952.
2. Hoff, N. J.; and Bruce, V. G.: "Dynamic Analysis of the Buckling of Laterally Loaded Flat Arches," Journal of Mathematics and Physics, Vol. 23, Jan. 1954, pp. 276-288.
3. Humphreys, J. S.: "On Dynamic Snap-Buckling of Shallow Arches," AIAA Journal, Vol. 4, No. 5, May 1966.
4. Lock, M. H.: "Snapping and Buckling Under Dynamic Pulse Load," AIAA Seventh Aerospace Sciences Meeting, Jan. 1969.
5. Lock, M. H.: "Snapping of a Shallow Sinusoidal Arch Under a Step Pressure Cord," AIAA Journal, Vol. 4, No. 7, July 1966.
6. Fulton, R. E.; and Barton, F. W.: "Dynamic Buckling of Shallow Arches," EMD Specialty Conference, Raleigh, N.C., Nov. 1967.
7. McCullers, L. A.: "Static and Dynamic Analysis of the Buckling of Shallow Arches," Master's Thesis, Department of Civil Engineering, Duke University, 1967.
8. Cheung, M. C.; and Babcock, C. D.: "An Energy Approach to the Dynamic Stability of Arches," AFDSR 69-2818TR, Sept. 1969.
9. Cheung, M. C.: "The Static and Dynamic Stability of Clamped Shallow Circular Arches," Ph.D. Dissertation, Department of Aeronautics, California Institute of Technology, 1969.
10. Simitzes, G. J.: "Dynamic Snap-Through Buckling of Low Arches and Shallow Spherical Cups," Ph.D. Dissertation, Department of Aeronautics and Astronautics, Stanford University, 1965.
11. Vahidi, B.: "Some Aspects of Dynamic Snap-Through Problems," Ph.D. Dissertation, Department of Applied Mechanics, University of California, San Diego, 1969.
12. Schreyer, H. L.; and Masur, E. F.: "Buckling of Shallow Arches," J. Eng. Mech. Div., Proc. ASCE, Vol. 85, No. EM 3, 1959.
13. Hoff, N. J.: "Dynamic Stability of Structures," Dynamic Stability of Structures, edited by George Herrmann, Pergamon Press, 1967.

14. Newmark, N. M.: "A Method of Computation for Structural Dynamics," Journal Engineering Mech. Div., Proc. ASCE, Vol. 85, No. EM 3, 1959.
15. Hildebrand, F. B.: Introduction to Numerical Analysis. McGraw-Hill, 1956, p. 451.
16. Hsu, C. S.: "The Effects of Various Parameters on the Dynamic Stability of a Shallow Arch," Journal of Applied Mechanics, Vol. 34, No. 2, June 1967.
17. Hsu, C. S.: "Stability of Shallow Arches Against Snap-Through Under Timewise Step Loads," Journal of Applied Mechanics, Vol. 35, No. 1, March 1968.
18. Hegemier, G. A.; and Tzung, F.: "Influence of Damping on the Snapping of a Shallow Arch Under a Step Pressure Load," AIAA Journal, Vol. 7, No. 8, August 1969.

TABLE 1.- CRITICAL STATIC LOADS

| <u>Arch geometry</u> | <u>Symmetric</u> |                 | <u>Asymmetric</u> |                 |
|----------------------|------------------|-----------------|-------------------|-----------------|
|                      | <u>Present</u>   | <u>Ref. [1]</u> | <u>Present</u>    | <u>Ref. [1]</u> |
| <u>e</u>             |                  |                 |                   |                 |
| 4.5                  | 9.00             | 8.48            | ---               | ---             |
| 5.0                  | 12.00            | 11.20           | ---               | 10.99           |
| 5.5                  | 15.00            | 14.48           | 13.16             | 13.21           |
| 6.0                  | 18.00            | 18.39           | 15.14             | 15.24           |
| 6.5                  | 22.00            | 22.98           | 16.97             | 17.17           |
| 7.0                  | 26.00            | 28.31           | 18.76             | 19.03           |
| 7.5                  | 29.00            | 34.43           | 20.53             | 20.83           |
| 8.0                  | 32.00            | 41.41           | 22.24             | 22.60           |
| 8.5                  | 36.00            | 49.29           | 23.94             | 24.34           |
| 9.0                  | 39.00            | 58.13           | 25.63             | 26.06           |
| 9.5                  | 42.00            | 68.00           | 27.27             | 27.76           |
| 10.0                 | 45.00            | 78.94           | 28.92             | 29.44           |
| 10.5                 | 48.00            | 91.02           | 30.57             | 31.12           |
| 11.0                 | 50.00            | 104.28          | 32.18             | 32.78           |
| 11.5                 | 53.00            | 118.80          | 33.81             | 34.43           |
| 12.0                 | 56.00            | 134.61          |                   | 36.08           |

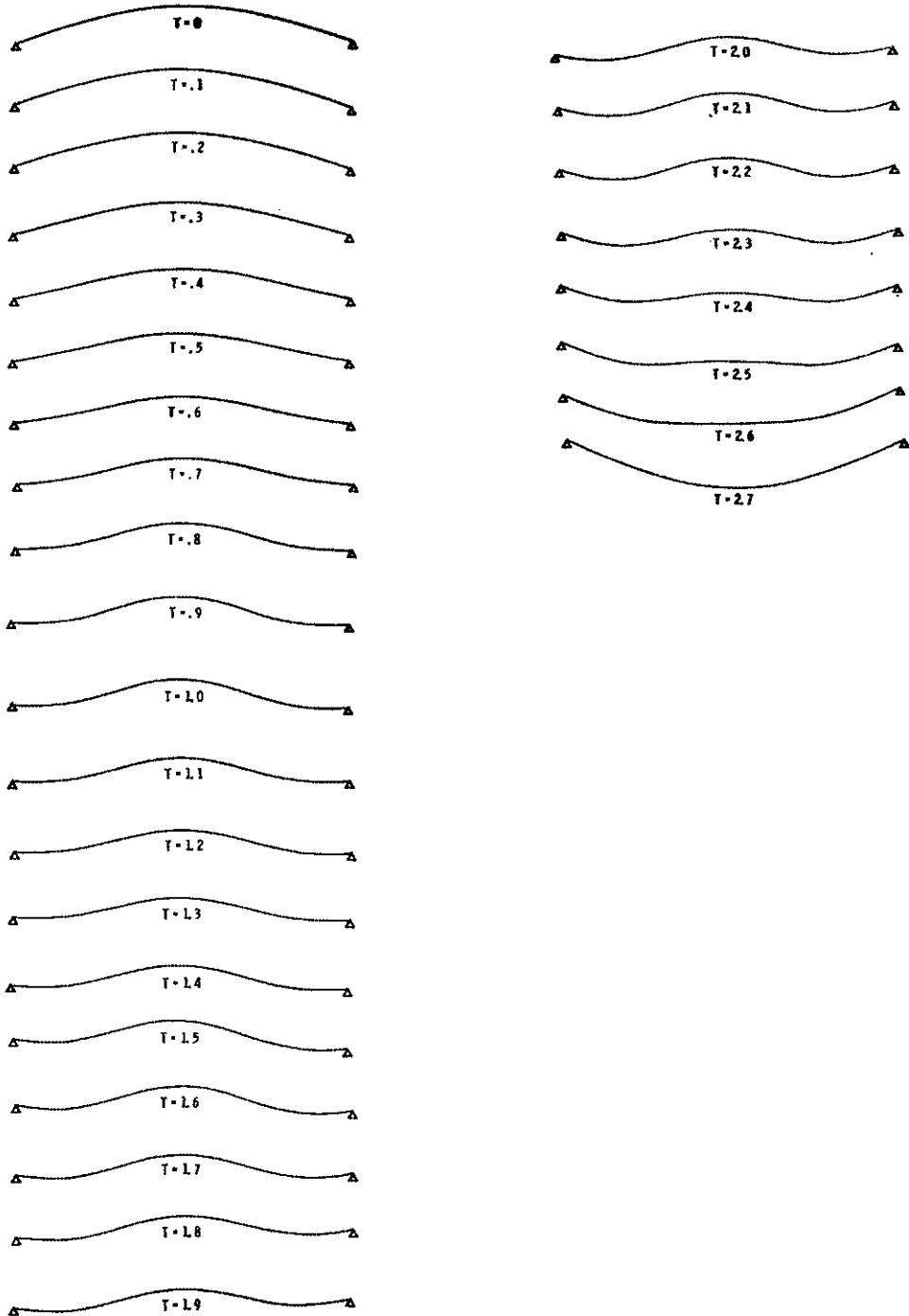
TABLE 2.- CRITICAL DYNAMIC LOADS - 0 PERCENT DAMPING

| <u>Arch geometry</u> | <u>Symmetric</u> |            | <u>Asymmetric</u> |            | <u>Delayed snapping</u> |            |
|----------------------|------------------|------------|-------------------|------------|-------------------------|------------|
|                      | <u>UNIF</u>      | <u>IMP</u> | <u>UNIF</u>       | <u>IMP</u> | <u>UNIF</u>             | <u>IMP</u> |
| e                    |                  |            |                   |            |                         |            |
| 4.5                  | 6.00             | 6.80       | 5.0 - D.S.        | 3.4        | ---                     |            |
| 5.0                  | 8.00             | 8.00       | 5.0 - D.S.        | 2.         | 8.2                     |            |
| 5.5                  | 11.00            | 9.20       | 8.0 - D.S.        | 8.         | 9.5                     |            |
| 6.0                  | 13.00            | 10.80      | 9.0 - D.S.        | 6.6        | 11.1                    |            |
| 6.5                  | 16.00            | 12.20      | 9.0 - D.S.        |            | 12.6                    | 10.        |
| 7.0                  | 19.00            | 13.60      | 9.0 - D.S.        | 5.2        | 14.1                    | 11.7       |
| 7.5                  | 22.00            | 15.00      | 9.0 - D.S.        | 4.6        | 15.7                    | 12.5       |
| 8.0                  | 25.00            | 16.60      | 8.0 - D.S.        | 4.0        | 17.5                    | 13.4       |
| 8.5                  | 28.00            | 18.20      | 8.0 - D.S.        | 3.0        | 18.8                    | 14.5       |
| 9.0                  | 31.00            | 19.60      | 7.0 - D.S.        | 2.6        | 20.4                    | 15.3       |
| 9.5                  | 34.00            | 21.20      |                   | 2.         |                         | 16.4       |
| 10.0                 | 37.00            | 23.00      | 4.0 - 19.0        | 2.         | 27.                     | 17.5       |
| 10.5                 | 40.00            | 24.60      | 2.0 - 11.0        | 1.         | 30.                     | 19.0       |
| 11.0                 | 43.00            | 26.40      |                   | 0          | 33.8                    | 20.        |
| 11.5                 | 46.00            | 28.00      |                   | 0          | 35.6                    | 20.        |
| 12.0                 | 49.00            | 29.80      |                   | 1.         | 37.1                    | 22.        |

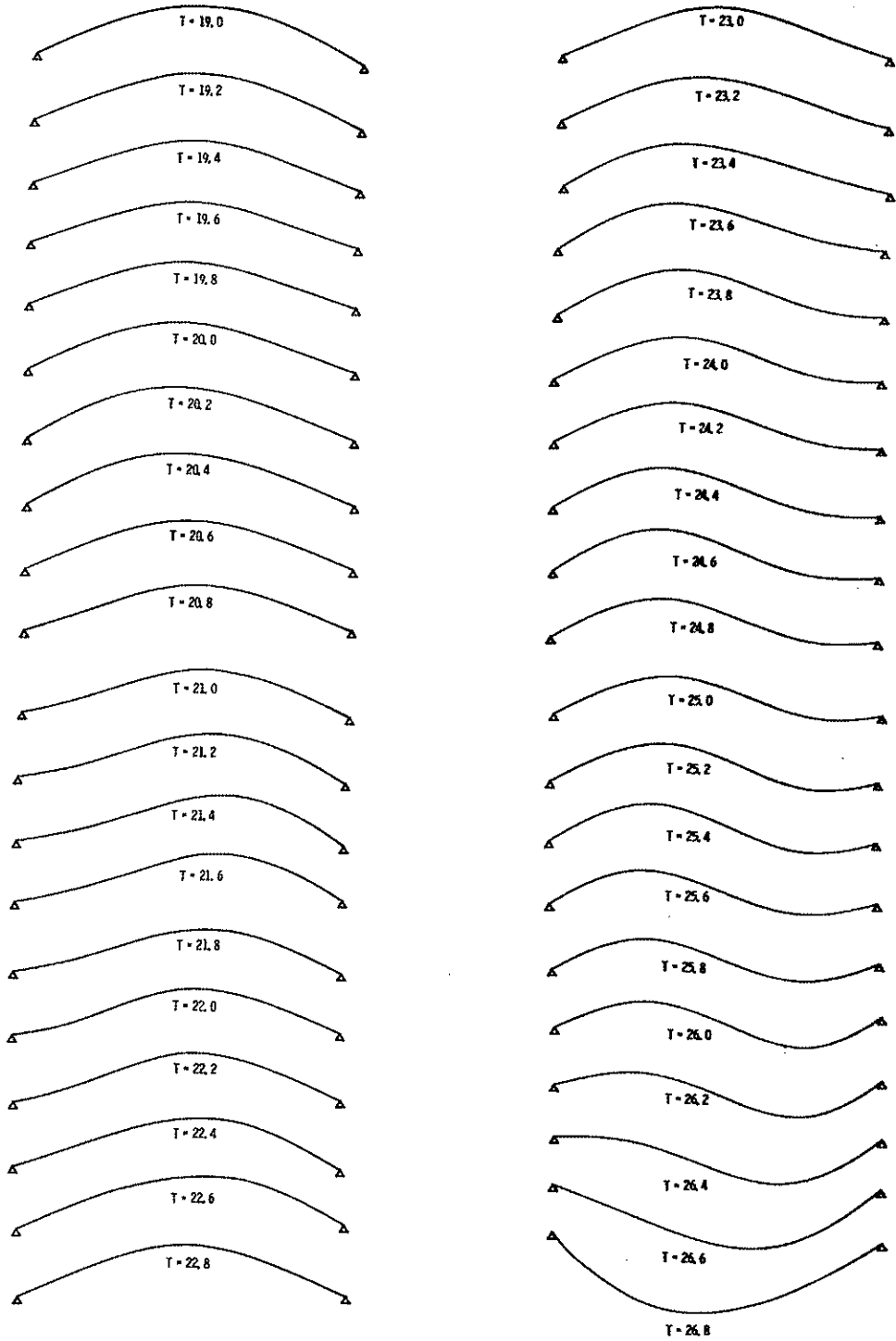
D.S. - Delayed Snapping

## APPENDIX 1

## Symmetric response configurations



## Asymmetric response configurations



## APPENDIX 2

Fortran IV program for static analysis

```

PROGRAM STBUCK(INPUT,OUTPUT,TAPE5=INPUT,TAPE6=OUTPUT)
C
C THIS IS A FORTRAN IV PROGRAM PRESENTLY
C SET UP TO CALCULATE CRITICAL SYMMETRIC
C AND ASYMMETRIC BUCKLING LOADS OF
C SHALLOW ARCHES USING A NEWTON-RAPHSON
C PROCEDURE. WITH SLIGHT MODIFICATION
C IT MAY ALSO BE USED TO DETERMINE
C EQUILIBRIUM PATHS OF THE LOAD
C DEFLECTION CURVE.
C
C
C INTEGER OUT
C REAL NX
C EXTERNAL FUNCT,FUNCL
C DIMENSION NAME(4)
C DIMENSION EQUA(15)
C DIMENSION WOXX(15),WO(15),F(11,11),G(11,1)
C DIMENSION IPIVOT(11)
C COMMON PI,NX,W(15),WX(15),WOX(15),Q(15)
C
C NAME = TITLE
C E = ARCH RISE
C EN = NUMBER OF INTERIOR FINITE DIFFERENCE STATIONS
C QL = INITIAL LOAD
C QINC = LOAD INCREMENT
C QF = FINAL LOAD
C EPS1 = TOLERANCE FACTOR
C S2B = BEGINNING FACTOR FOR ANTISYMMETRIC COMPONENT
C S2E = END FACTOR FOR ANTISYMMETRIC COMPONENT
C S2INC = INCREMENT FOR ANTISYMMETRIC FACTOR
C S3B = BEGINNING FACTOR FOR THIRD MODE COMPONENT
C S3E = END FACTOR FOR THIRD MODE COMPONENT
C S3UNC = INCREMENT FOR THIRD MODE FACTOR
C ID2 = 1 DECREMENT THE LOAD
C ID2 = 2 INCREMENT THE LOAD
C ID5 = 1 NORMAL SOLUTION
C ID5 = 2 SYMMETRIC BUCKLING LOAD ONLY
C ID6 = 1 INCREMENT ON THIRD MODE COMPONENT
C ID6 = 2 INCREMENT ON ANTISYMMETRIC COMPONENT
C
C
C READ 500,NAME
500 FORMAT(4A10)

```

```

      PRINT 82,NAME
82  FORMAT(1H1,4A10)
      CON = 0.
      ID2 = 2
      ID3 = 1
      ID5 = 1
      ID6 = 2
      READ 1,E,EN,QL,QINC,EPS1,QF
      READ 1,S2B,S2E,S2INC,S3B,S3E,S3INC
1  FORMAT(6F10.5)

```

```

C
C      INITIALIZATION OF PROGRAM PARAMETERS
C

```

```

      N = EN
      PI = 3.1415926536
      DX = PI/(EN-1.)
      ICR = (N+3)/2
16  CONTINUE
      X1S = 0.
      X2S = 0.
      Y1S = 0.
      Y2S = 0.
      X1AS = 0.
      X2AS = 0.
      Y1AS = 0.
      Y2AS = 0.
      IBIFIR = 1
      IWAV = 0
      S2 = 0.
      S3 = 0.
35  CONTINUE
      DISL = 0.
      J = N+1
      DO 13 I = 2,J
      EQUA(I) = 0.
      WQ(I) = 0.
      WOX(I) = 0.
      WOX (I) = 0.
      Q(I)=QL
      WX(I) = 0.
13  W(I) = C.
      DO 17 I=1,11
      DO 17 M=1,11

```

```

17 F(I,M) = 0.
   DO 18 I=1,11
18 G(I) = C.
C
C   BOUNCARY CONDITIONS
C
   W(1) = -W(3)
   W(15) = -W(13)
C
C   INITIAL GECMETRY
C
   DO 2 I = 2,J
   AI=I-2
   WO(I) = -E*SIN(DX*AI)
   WOX(I) = -E*COS(DX*AI)
   WOXX(I) = -WO(I)
   W(I) = - CON*WO(I)
2 CONTINUE
61 CONTINUE
   IF(Q(ICR)-QF)80,80,81
81 S3B = S3B + S3INC
   S2B = S2B + S2INC
   GO TO 35
80 CONTINUE
40 CONTINUE
C
C   BEGIN NEWTON-RAPHSON PROCEDURE
C
   W(1) = -W(3)
   W(N+2) = -W(N)
   DO 3 I = 2,J
3 WX(I) = (1./(2.*DX))*(-W(I-1)+W(I+1))
C
C   CALCULATION OF NX
C
   CALL SIMP(DX,N,FUNCT,NX)
C
C   MATRIX SETUP FOR SOLUTION
C
   CALL MATSI(PI,NX,DX,W,WOX,WXX,F,G,Q)
C
C   SOLUTION OF MATRIX EQUATIENS
C

```

```

      CALL SIMEQ(F,11,G,1 ,DETERM,IPIVOT,11,ISCALE)
C
C   TOLERANCE CHECK
C
      DO 8 II = 1,11
      A = ABS(G(II,1))
      IF(A-EPS1)8,8,9
C
C   CORRECTION OF ASSUMED DEFLECTED SHAPE
C
      9 DO 11 I=1,11
      W(I+2) = W(I+2)+G(I)
11 CONTINUE
      GO TO 40
      8 CONTINUE
C
C   NEWTON-RAPHSON SOLUTION COMPLETE FOR
C   GIVEN LOAD AND INITIAL GEOMETRY
C
      W(1) = -W(3)
      W(N+2) = -W(N)
C
C   CALCULATION OF AVERAGE DEFLECTION
C
      CALL SIMP(DX,N,FUNC1,WAV)
      QD = Q(ICR)
      WAV = WAV/PI
C
C   THE FOLLOWING PART OF THE PROGRAM
C   DETERMINES WHICH EQUILBRIUM BRANCH
C   THE SOLUTION HAS CONVERGED ON.
C   AFTER TWO SOLUTIONS HAVE BEEN
C   OBTAINED FOR THE ASYMMETRIC BRANCH
C   THE PROGRAM THEN PROCEEDS TO FIND
C   THE CRITICAL SYMMETRIC LOAD WITHOUT
C   STORING ANYMORE ASYMMETRIC POINTS
C
      IF(IWAV)12,4,12
      4 IF(WAV.GT.1.3*E) GO TO 15
      WAVB = WAV
      IWAV = 1
12 CONTINUE
      IF(ABS(WAVB-WAV).GT.10.E-4.AND.WAV.LT.1.3*E.AND.IBIFIR.LT.3)

```

```
1 GO TO 14
GO TO 24
14 IF(IBIFIR.EQ.1) GO TO 19
X2S = WAVB
Y2S = Q(ICR)
X2AS = WAV
Y2AS = Q(ICR)
GO TO 20
19 X1S = WAVB
Y1S = Q(ICR)
X1AS = WAV
Y1AS = Q(ICR)
20 CONTINUE
IBIFIR = IBIFIR + 1
24 CONTINUE
GO TO (50,51),ID5
50 IF(S2)52,53,52
53 IF(S3)52,54,52
54 S1 = W(ICR)
52 CONTINUE
GO TO (64,65),ID6
65 IF(S2-S2E)55,56,56
55 S2 = S2 + S2INC
S3 = S3B
GO TO 66
64 IF(S3-S3E)63,56,56
63 S3 = S3 + S3INC
S2 = S2B
66 DO 57 I = 2,14
AI = I-2
W(I)=S1*SIN(AI*DX)+S2*SIN(2.*AI*DX)+S3*SIN(3.*AI*DX)
57 CONTINUE
GO TO 61
56 DO 58 I = 2,14
AI = I-2
W(I) = S1*SIN(AI*DX)
58 CONTINUE
S2 = 0.
S3 = 0.
IWAV = 0
51 CONTINUE
GO TO (30,29),ID2
29 DO 5 I=2,14
```

```

5 Q(I) = Q(I) + QTNC
  GO TO 10
30 DO 31 I = 2,14
31 Q(I) = Q(I) - QTNC
10 CONTINUE
  GO TO 61
15 CONTINUE

C
C   OUTPUT
C
C   IF(X1S.EQ.0..OR.X2S.EQ.0.) GO TO 22
C
C   CALCULATION OF CRITICAL ASYMMETRIC
C   LOAD FROM THE TWO POINTS OBTAINED
C   ABOVE
C
  AIS = Y2S-Y1S
  BIS = X2S-X1S
  CIS = X2S*Y1S - X1S*Y2S
  AIAS = Y2AS-Y1AS
  BIAS = X2AS-X1AS
  CIAS = X2AS*Y1AS-X1AS*Y2AS
  QAS = (AIAS*CIS-CIAS*AIS)/(AIAS*BIS-BIAS*AIS)
  PRINT 123,E,QAS,QO
123 FORMAT(* FOR AN ARCH RISE OF *F5.1* THE CRITICAL ANTISYM LOAD IS *
  IF10.4* AND THE CRITICAL SYMM LOAD IS *F8.3)
  GO TO 23
22 PRINT 122,E,QO
122 FORMAT(* FOR AN ARCH RISE OF *F5.1* THE CRITICAL ANTISYM LOAD IS U
  INDEFINED AND THE CRITICAL SYMM LOAD IS *F8.3)
23 CONTINUE
  E = E + .5
  IF(E.GT.12.) STOP
  GO TO 16

END

```

```
FUNCTION FUNCT(I)  
C  
C FUNCT IS USED IN SIMP TO CALCULATE  
C THE AXIAL FORCE NX  
C  
COMMON PI,NX,W(15),WX(15),WOX(15),O(15)  
FUNCT=(1./(2.*PI))*(2.*WOX(I)*WX(I)+WX(I)*WX(I))  
RETURN  
END
```

```
FUNCTION FUNC1(I)  
C  
C   FUNC1 IS USED IN SIMP TO CALCULATE  
C   AN AVERAGE DEFLECTION  
C  
COMMON PI,NX,W(15),WX(15),WOX(15),Q(15)  
FUNC1 = W(I)  
RETURN  
END
```

```
      SUBROUTINE SIMP(H,N,FUNCT,ANS)
C
C   THE SUBROUTINE SIMP PROVIDES THE
C   NUMERICAL INTEGRATION TECHNIQUE
C
      DIMENSION Y(15)
      N3=N+1
      DO 1 I=2,N3
1     Y(I)=FUNCT(I)
      ANS1=0.0
      DO 2 I=3,N,2
2     ANS1=ANS1+4.*Y(I)
      N2=N-1
      ANS2=0.0
      DO 3 I=4,N2,2
3     ANS2=ANS2+2.*Y(I)
      ANS=H*(Y(2)+ANS1+ANS2+Y(N3))/3.
      RETURN
      END
```

```

SUBROUTINE MATS1(PI,NX,DX,W,WOX,WOXX,F,G,Q)
C
C THE SUBROUTINE MATS1 SETS UP THE
C ENTIRE SET OF MATRIX EQUATIONS
C NEEDED IN THE NEWTON-RAPHSON PROCEDURE
C   PNXI = PARTIAL OF NX WRT W(I)
C   F(I,J) = PARTIAL OF F(I) WRT W(J)
C       I = 1,2,3,...N
C       J = 3,4,5,...N+2
C   G(I,1) = -F(I)
C
REAL NX
DIMENSION W(15),WOX(15),WCXX(15),CFM(15),F(11,11),G(11,1),Q(15)
DEL2 = DX*DX
CF1 = 4. + NX*DEL2
CF2 = 6. + 2.*NX*DEL2
CF3 = 5. + 2.*NX*DEL2
CF5 = NX*DEL2*DEL2
CF7 = DEL2*(2.*W(3)-W(4)-DEL2*WOXX(3))
CFMM=DEL2*(-W(12)+2.*W(13)-DEL2*WOXX(13))
DO 1 I=3,11
1 CFM(I) = DEL2*(-W(I)+2.*W(I+1)-W(I+2)-DEL2*WOXX(I+1))
CF9=1./(6.*PI)
CF10=1./(3.*PI)
G(1,1) = -(CF3*W(3)-CF1*W(4)+W(5)-CF5*WOXX(3)-Q(3)*DEL2**2)
G(2,1) = -(CF1*W(3)+CF2*W(4)-CF1*W(5)+W(6)-CF5*WOXX(4)-Q(4)*DEL2**2)
1)
G(3,1) = -(W(3)-CF1*W(4)+CF2*W(5)-CF1*W(6)+W(7)-CF5*WOXX(5)-Q(5)*DEL2**2)
G(4,1) = -(W(4)-CF1*W(5)+CF2*W(6)-CF1*W(7)+W(8)-CF5*WOXX(6)-Q(6)*DEL2**2)
G(5,1) = -(W(5)-CF1*W(6)+CF2*W(7)-CF1*W(8)+W(9)-CF5*WOXX(7)-Q(7)*DEL2**2)
G(6,1) = -(W(6)-CF1*W(7)+CF2*W(8)-CF1*W(9)+W(10)-CF5*WOXX(8)-Q(8)*DEL2**2)
G(7,1) = -(W(7)-CF1*W(8)+CF2*W(9)-CF1*W(10)+W(11)-CF5*WOXX(9)-Q(9)*DEL2**2)
G(8,1) = -(W(8)-CF1*W(9)+CF2*W(10)-CF1*W(11)+W(12)-CF5*WOXX(10)-Q(10)*DEL2**2)
G(9,1) = -(W(9)-CF1*W(10)+CF2*W(11)-CF1*W(12)+W(13)-CF5*WOXX(11)-Q(11)*DEL2**2)
G(10,1) = -(W(10)-CF1*W(11)+CF2*W(12)-CF1*W(13)-CF5*WOXX(12)-Q(12)

```

```

1*DEL2**2)
G(11,1) = -(W(11)-CF1*W(12)+(CF2-1.)*W(13)-CF5*W(13)-Q(13)*DEL2
1**2)
PNX3=CF9*(2.*(WOX(2)-WDX(4))+(3.*W(3)-W(5))/DX)
PNX4=CF10*(2.*WOX(3)-2.*WOX(5)+(2.*W(4)-W(6))/DX)
PNX5 = CF9*(2.*(WOX(4)-WDX(6))+(2.*W(5)-W(3)-W(7))/DX)
PNX6 = CF10*(2.*(WOX(5)-WDX(7))+(2.*W(6)-W(4)-W(8))/DX)
PNX7 = CF9*(2.*WOX(6)+(W(7)-W(5))/DX)
PNX8=CF10*(2.*(WOX(7)-WDX(9))+(2.*W(8)-W(6)-W(10))/DX)
PNX9=CF9*(2.*(WOX(8)-WDX(10))+(2.*W(9)-W(7)-W(11))/DX)
PNX10=CF10*(2.*(WOX(9)-WDX(11))+(2.*W(10)-W(8)-W(12))/DX)
PNX11=CF9*(2.*(WOX(10)-WDX(12))+(2.*W(11)-W(9)-W(13))/DX)
PNX12=CF10*(2.*(WOX(11)-WDX(13))+(2.*W(12)-W(10))/DX)
PNX13=CF9*(2.*(WOX(12)-WDX(14))+(3.*W(13)-W(11))/DX)
F(1,1)=CF7*PNX3+CF3
F(2,1)=CFM(3)*PNX3-CF1
F(3,1)=CFM(4)*PNX3+1.
F(4,1)=CFM(5)*PNX3
F(5,1)=CFM(6)*PNX3
F(6,1)=CFM(7)*PNX3
F(7,1)=CFM(8)*PNX3
F(8,1)=CFM(9)*PNX3
F(9,1)=CFM(10)*PNX3
F(10,1)=CFM(11)*PNX3
F(11,1)=CFMM*PNX3
F(1,2)=CF7*PNX4-CF1
F(2,2)=CFM(3)*PNX4+CF2
F(3,2)=CFM(4)*PNX4-CF1
F(4,2)=CFM(5)*PNX4+1.
F(5,2)=CFM(6)*PNX4
F(6,2)=CFM(7)*PNX4
F(7,2)=CFM(8)*PNX4
F(8,2)=CFM(9)*PNX4
F(9,2)=CFM(10)*PNX4
F(10,2)=CFM(11)*PNX4
F(11,2)=CFMM*PNX4
F(1,3)=CF7*PNX5+1.
F(2,3)=CFM(3)*PNX5-CF1
F(3,3)=CFM(4)*PNX5+CF2
F(4,3)=CFM(5)*PNX5-CF1
F(5,3)=CFM(6)*PNX5+1.
F(6,3)=CFM(7)*PNX5
F(7,3)=CFM(8)*PNX5

```

F(8,3)=CFM(9)\*PNX5  
F(9,3)=CFM(10)\*PNX5  
F(10,3)=CFM(11)\*PNX5  
F(11,3)=CFMM\*PNX5  
F(1,4)=CF7\*PNX6  
F(2,4)=CFM(3)\*PNX6+1.  
F(3,4)=CFM(4)\*PNX6-CF1  
F(4,4)=CFM(5)\*PNX6+CF2  
F(5,4)=CFM(6)\*PNX6-CF1  
F(6,4)=CFM(7)\*PNX6+1.  
F(7,4)=CFM(8)\*PNX6  
F(8,4)=CFM(9)\*PNX6  
F(9,4)=CFM(10)\*PNX6  
F(10,4)=CFM(11)\*PNX6  
F(11,4)=CFMM\*PNX6  
F(1,5)=CF7\*PNX7  
F(2,5)=CFM(3)\*PNX7  
F(3,5)=CFM(4)\*PNX7+1.  
F(4,5)=CFM(5)\*PNX7-CF1  
F(5,5)=CFM(6)\*PNX7+CF2  
F(6,5)=CFM(7)\*PNX7-CF1  
F(7,5)=CFM(8)\*PNX7+1.  
F(8,5)=CFM(9)\*PNX7  
F(9,5)=CFM(10)\*PNX7  
F(10,5)=CFM(11)\*PNX7  
F(11,5)=CFMM\*PNX7  
F(1,6)=CF7\*PNX8  
F(2,6)=CFM(3)\*PNX8  
F(3,6)=CFM(4)\*PNX8  
F(4,6)=CFM(5)\*PNX8+1.  
F(5,6)=CFM(6)\*PNX8-CF1  
F(6,6)=CFM(7)\*PNX8+CF2  
F(7,6)=CFM(8)\*PNX8-CF1  
F(8,6)=CFM(9)\*PNX8+1.  
F(9,6)=CFM(10)\*PNX8  
F(10,6)=CFM(11)\*PNX8  
F(11,6)=CFMM\*PNX8  
F(1,7)=CF7\*PNX9  
F(2,7)=CFM(3)\*PNX9  
F(3,7)=CFM(4)\*PNX9  
F(4,7)=CFM(5)\*PNX9  
F(5,7)=CFM(6)\*PNX9+1.  
F(6,7)=CFM(7)\*PNX9-CF1

$F(7,7)=CFM(8)*PNX9+CF2$   
 $F(8,7)=CFM(9)*PNX9-CF1$   
 $F(9,7)=CFM(10)*PNX9+1.$   
 $F(10,7)=CFM(11)*PNX9$   
 $F(11,7)=CFMM*PNX9$   
 $F(1,8)=CF7*PNX10$   
 $F(2,8)=CFM(3)*PNX10$   
 $F(3,8)=CFM(4)*PNX10$   
 $F(4,8)=CFM(5)*PNX10$   
 $F(5,8)=CFM(6)*PNX10$   
 $F(6,8)=CFM(7)*PNX10+1.$   
 $F(7,8)=CFM(8)*PNX10-CF1$   
 $F(8,8)=CFM(9)*PNX10+CF2$   
 $F(9,8)=CFM(10)*PNX10-CF1$   
 $F(10,8)=CFM(11)*PNX10+1.$   
 $F(11,8)=CFMM*PNX10$   
 $F(1,9)=CF7*PNX11$   
 $F(2,9)=CFM(3)*PNX11$   
 $F(3,9)=CFM(4)*PNX11$   
 $F(4,9)=CFM(5)*PNX11$   
 $F(5,9)=CFM(6)*PNX11$   
 $F(6,9)=CFM(7)*PNX11$   
 $F(7,9)=CFM(8)*PNX11+1.$   
 $F(8,9)=CFM(9)*PNX11-CF1$   
 $F(9,9)=CFM(10)*PNX11+CF2$   
 $F(10,9)=CFM(11)*PNX11-CF1$   
 $F(11,9)=CFMM*PNX11+1.$   
 $F(1,10)=CF7*PNX12$   
 $F(2,10)=CFM(3)*PNX12$   
 $F(3,10)=CFM(4)*PNX12$   
 $F(4,10)=CFM(5)*PNX12$   
 $F(5,10)=CFM(6)*PNX12$   
 $F(6,10)=CFM(7)*PNX12$   
 $F(7,10)=CFM(8)*PNX12$   
 $F(8,10)=CFM(9)*PNX12+1.$   
 $F(9,10)=CFM(10)*PNX12-CF1$   
 $F(10,10)=CFM(11)*PNX12+CF2$   
 $F(11,10)=CFMM*PNX12-CF1$   
 $F(1,11)=CF7*PNX13$   
 $F(2,11)=CFM(3)*PNX13$   
 $F(3,11)=CFM(4)*PNX13$   
 $F(4,11)=CFM(5)*PNX13$   
 $F(5,11)=CFM(6)*PNX13$

```
F(6,11)=CFM(7)*PNX13  
F(7,11)=CFM(8)*PNX13  
F(8,11)=CFM(9)*PNX13  
F(9,11)=CFM(10)*PNX13+1.  
F(10,11)=CFM(11)*PNX13-CF1  
F(11,11)=CFMM*PNX13+CF2-1.  
RETURN  
END
```

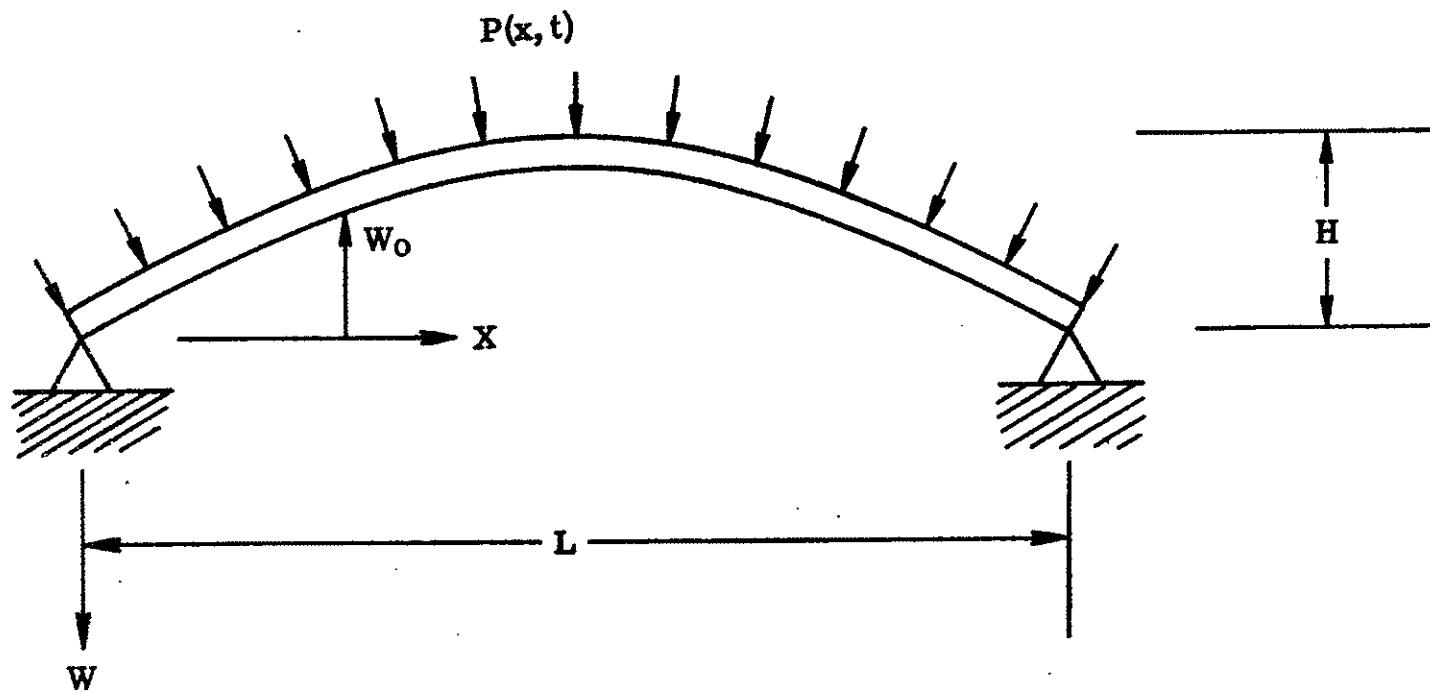


Figure 1.- Shallow arch.

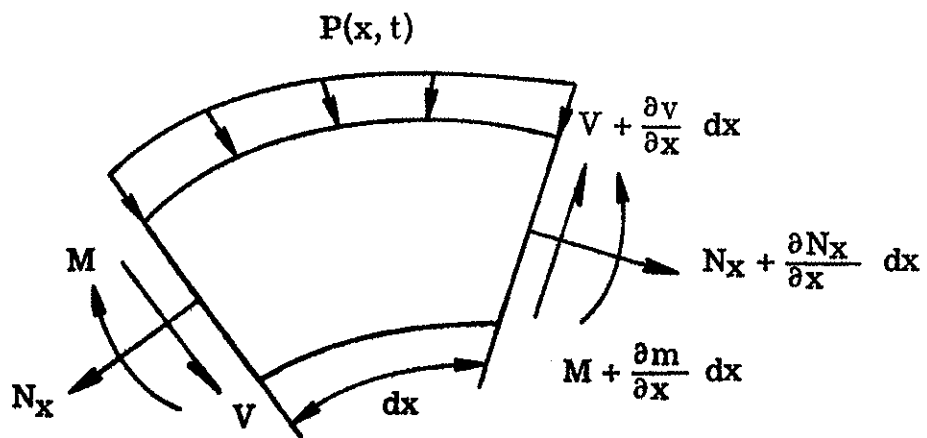


Figure 2.- Differential element.

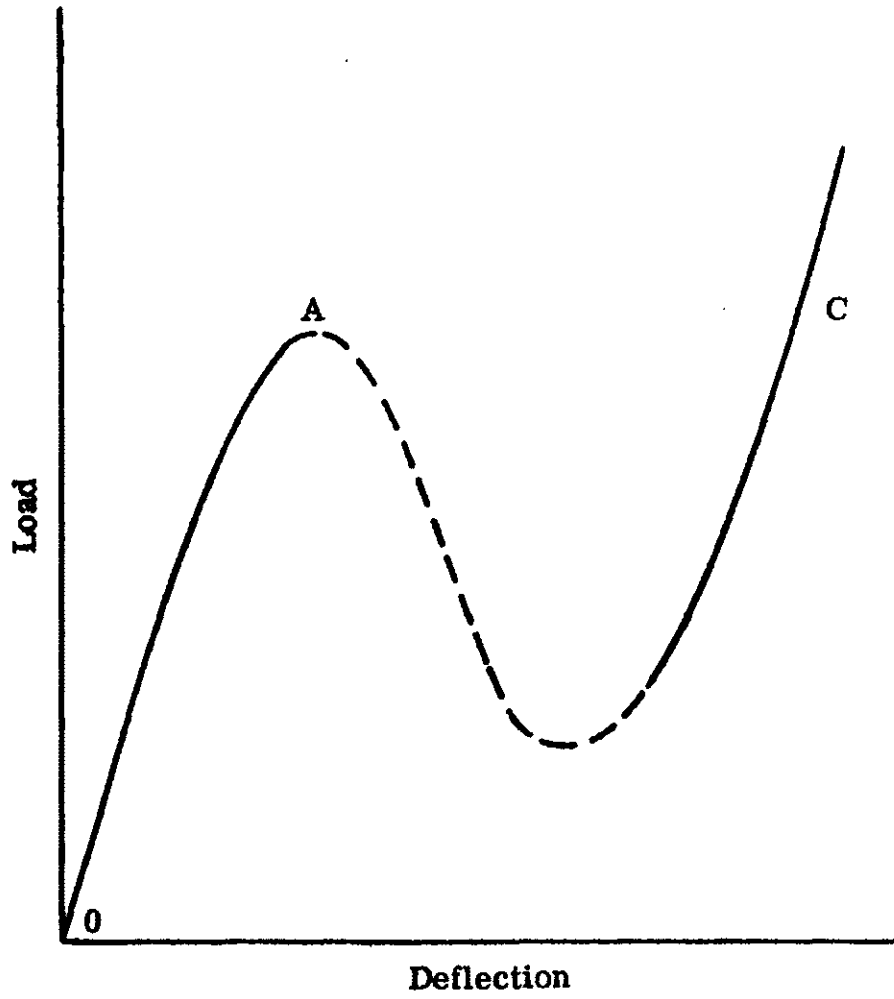


Figure 3.- Static load deflection curve.

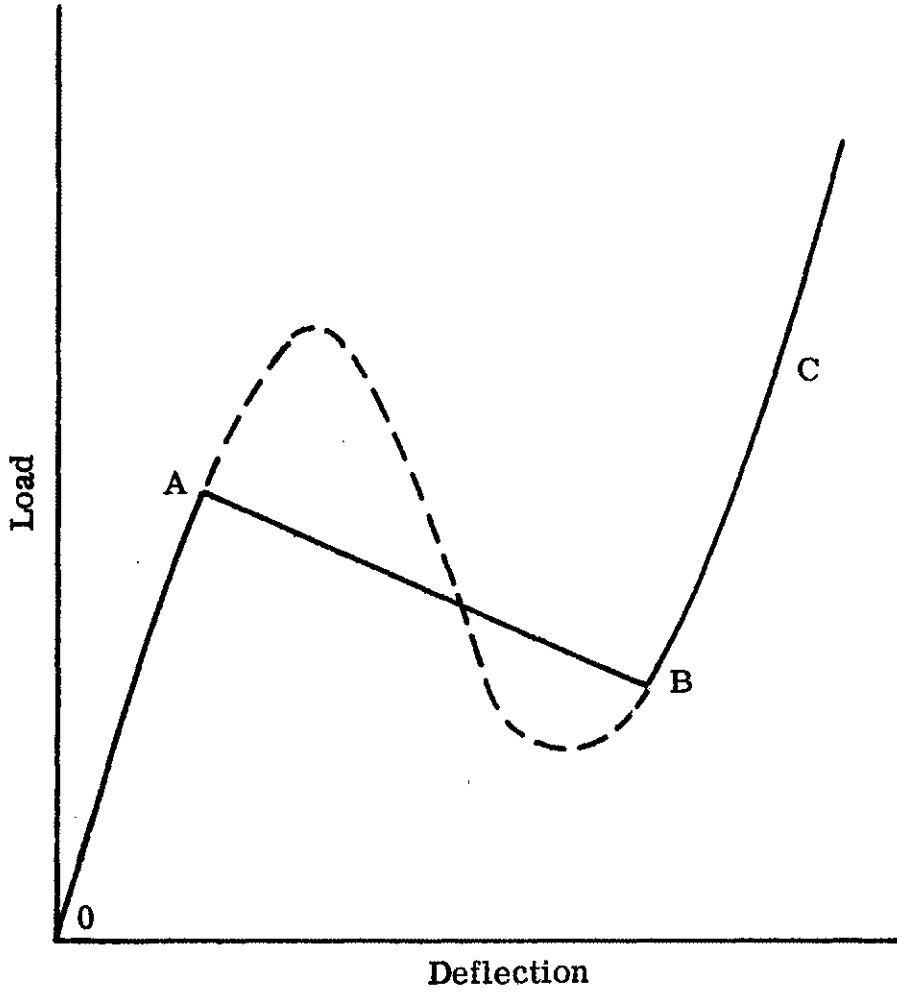


Figure 4.- Asymmetric static load deflection curve.

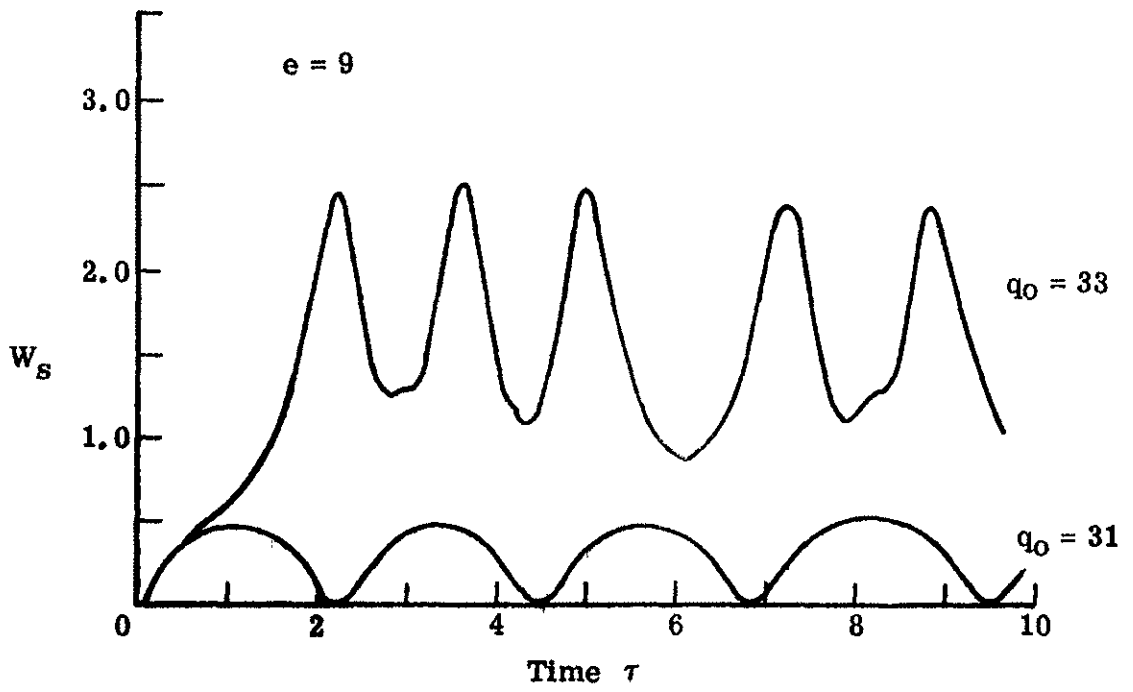


Figure 5.- Symmetric response.

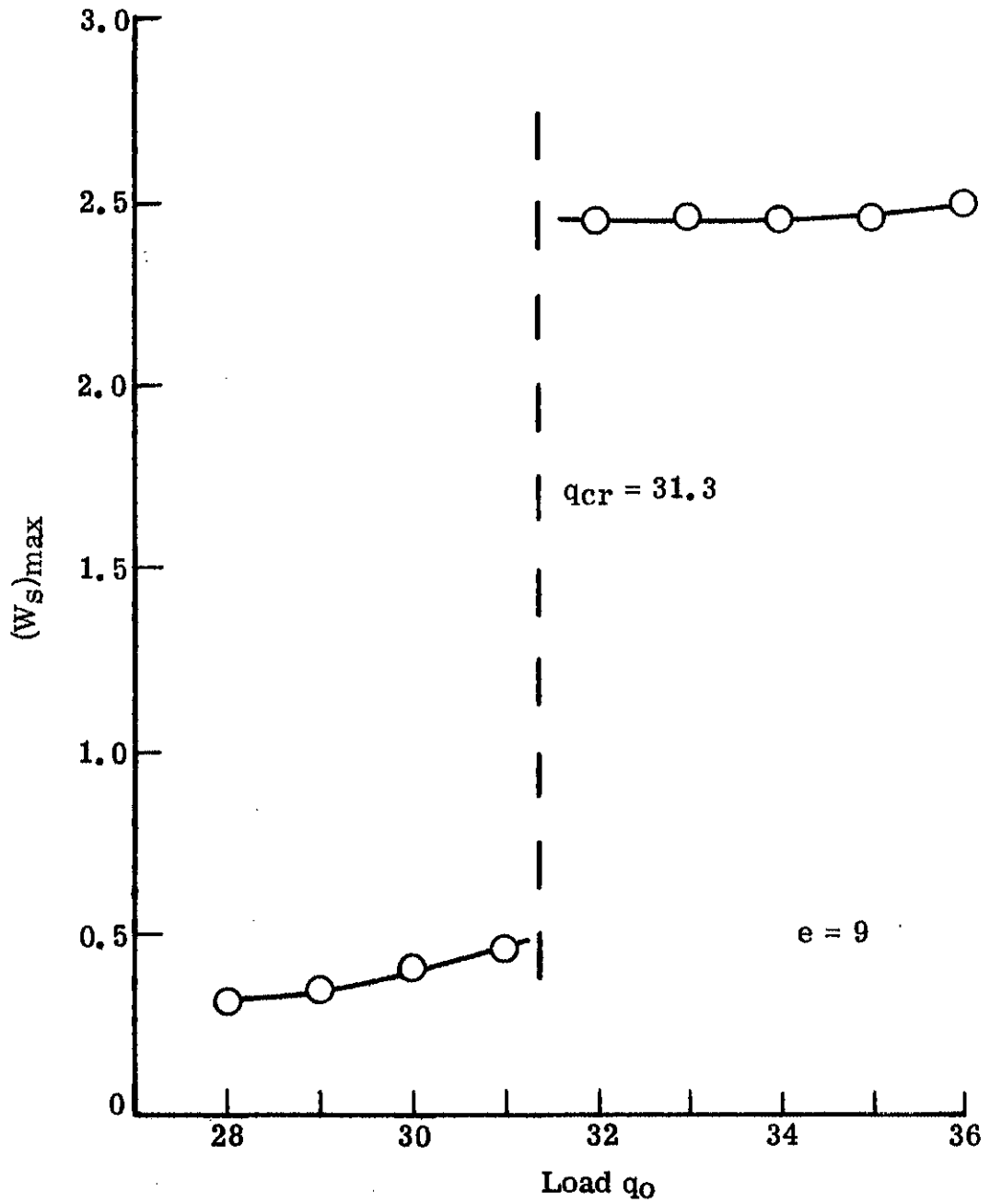


Figure 6.- Symmetric buckling criteria.

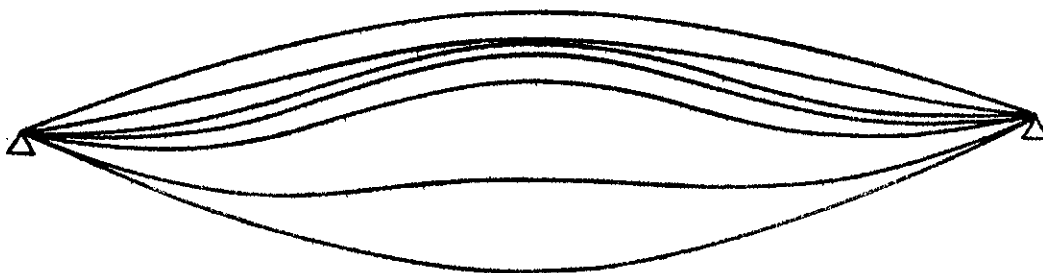


Figure 7.- Arch configurations during symmetric snap-through.

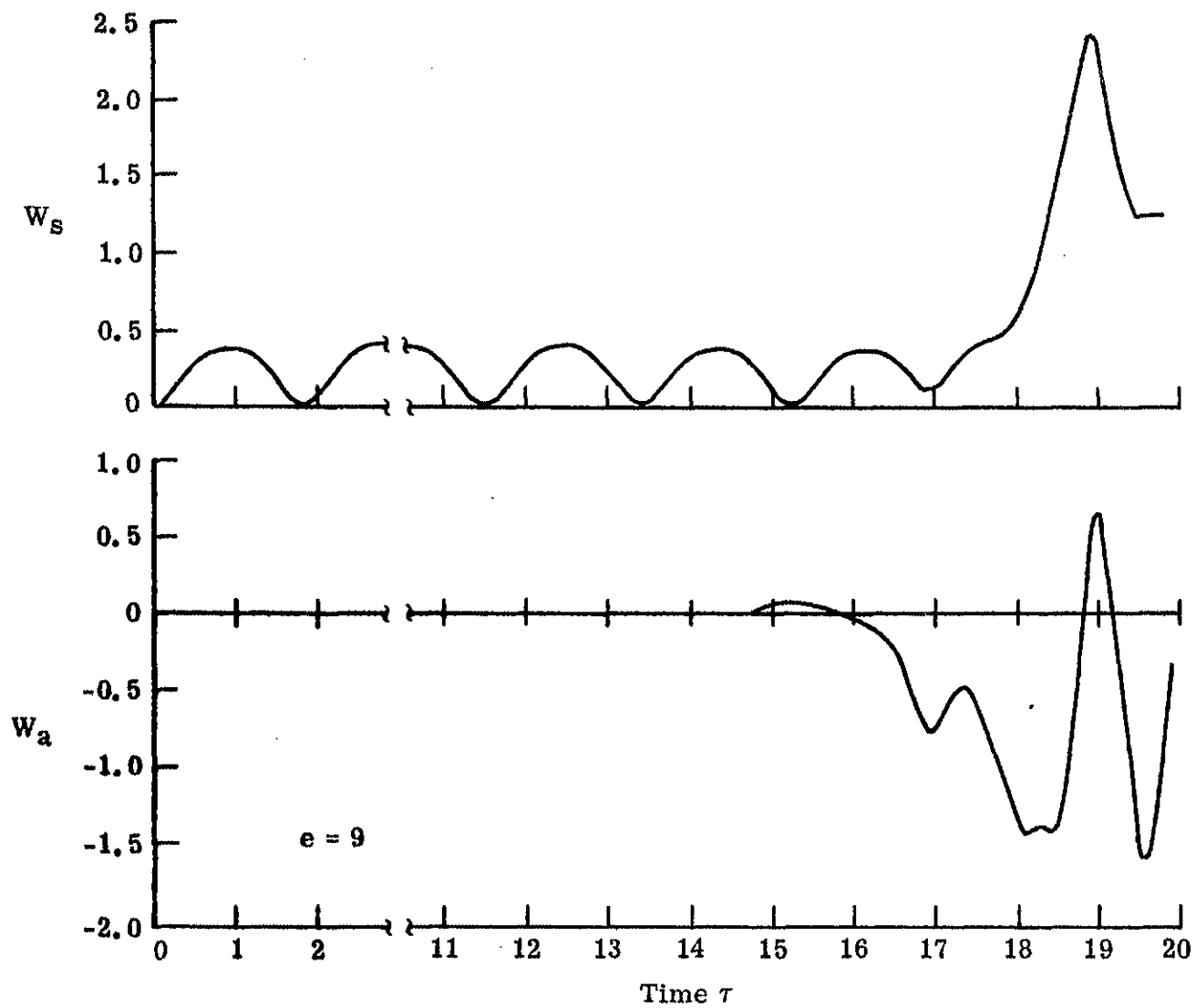


Figure 8.- Typical dynamic response.

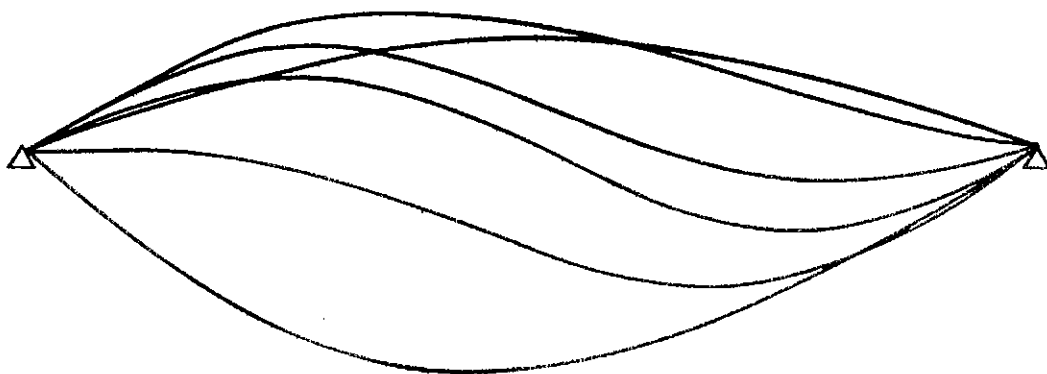


Figure 9.- Arch configurations during delayed snapping.

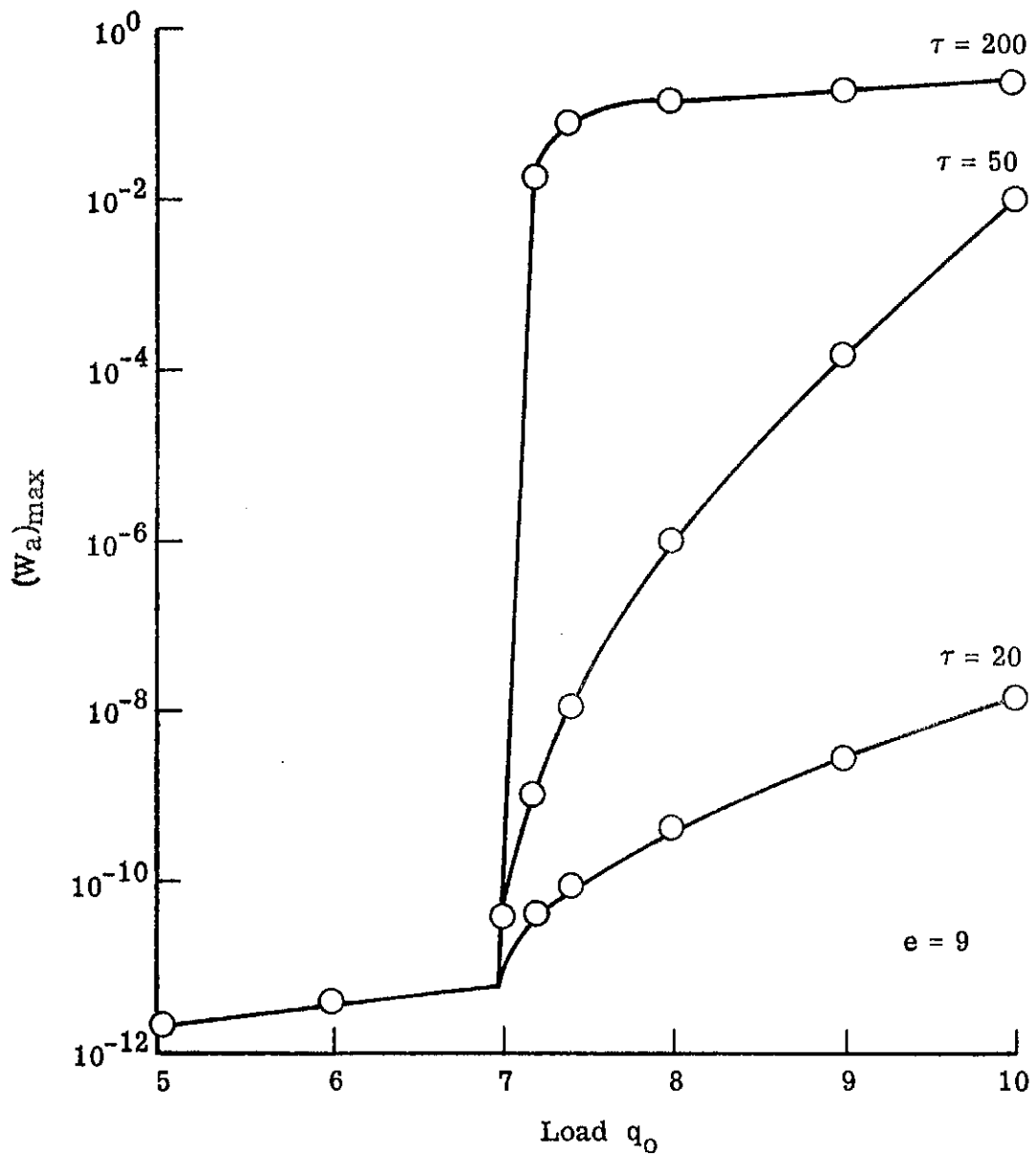


Figure 10. Asymmetric buckling criteria.

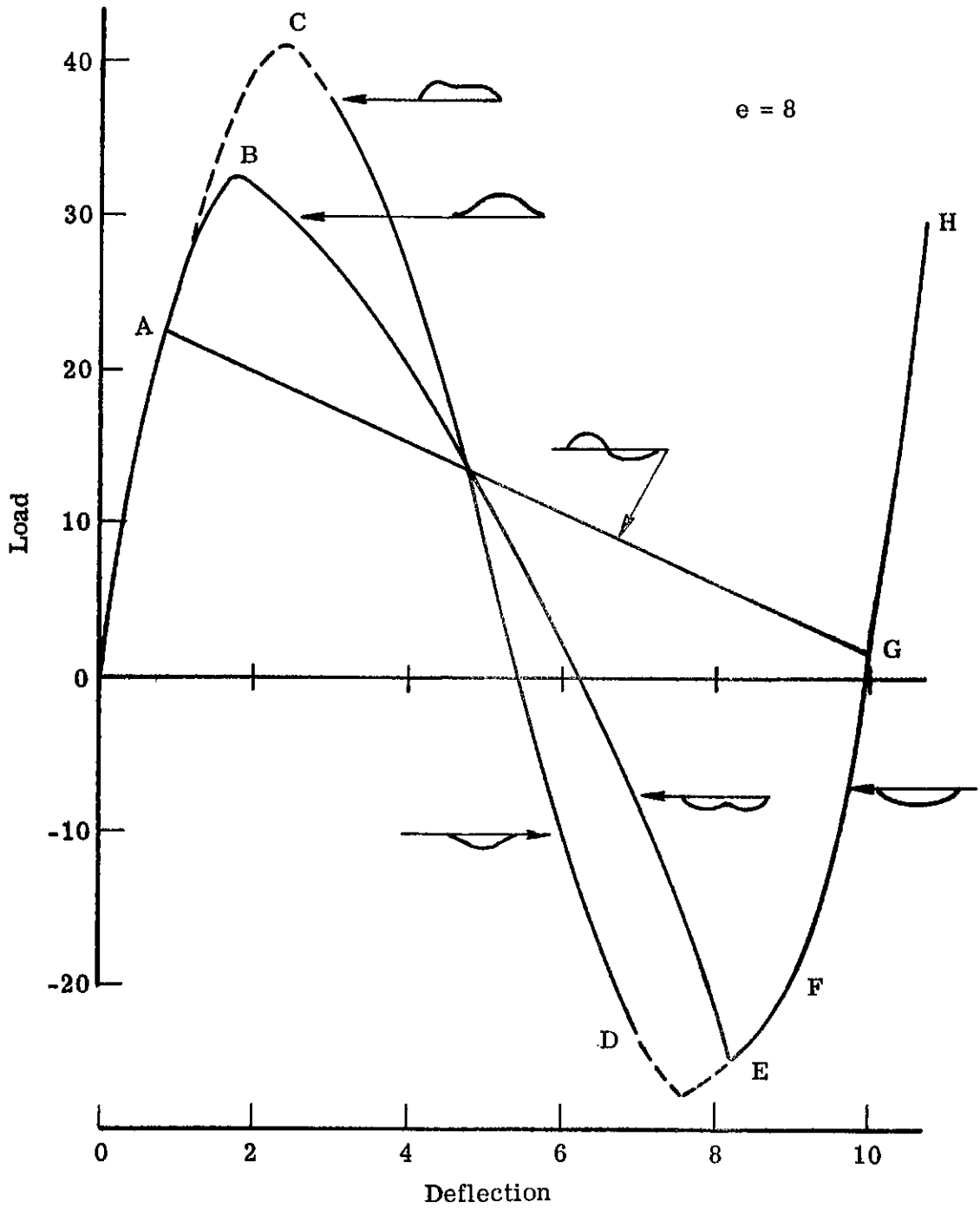


Figure 11.- Static stability curve.

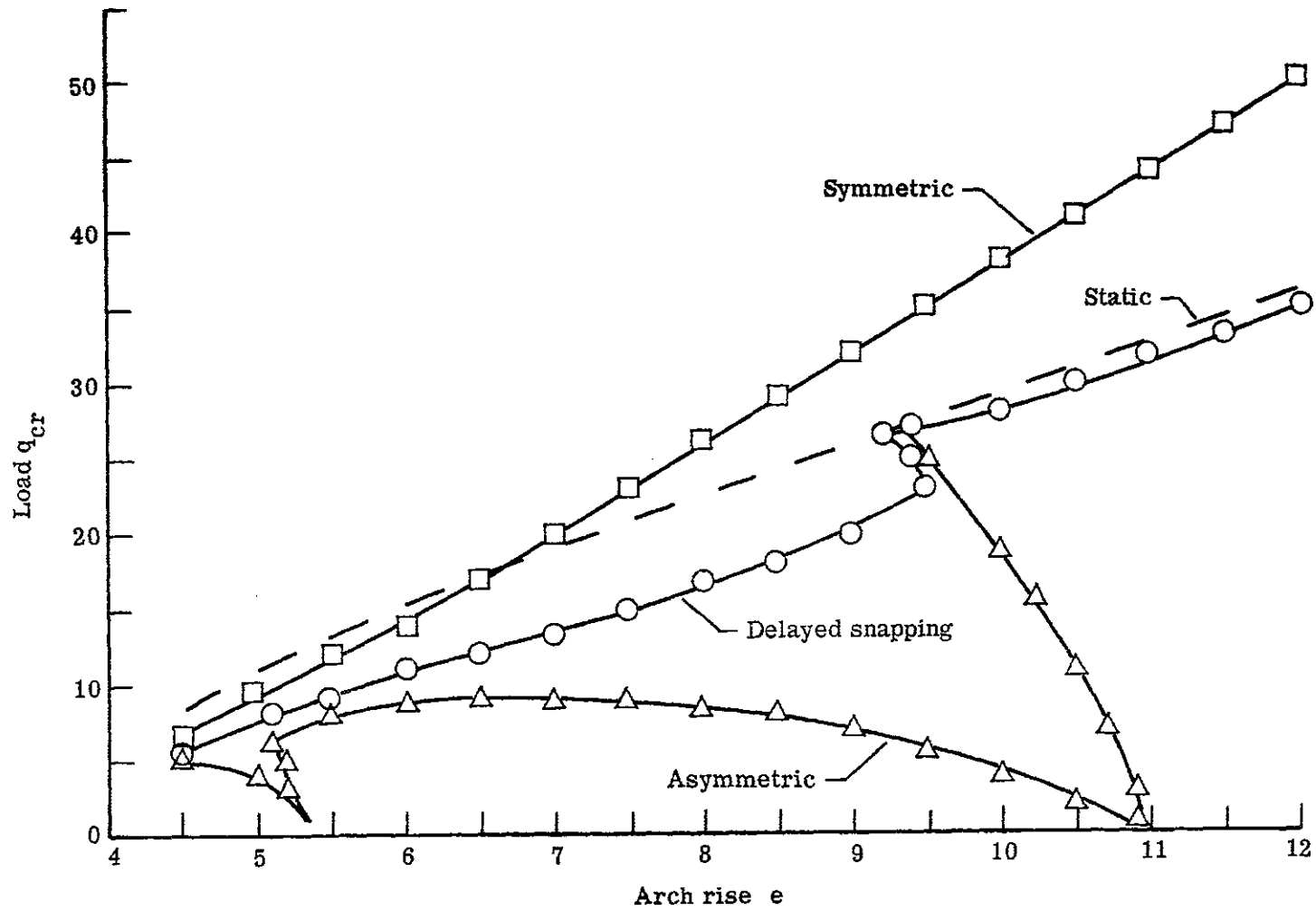


Figure 12.- Dynamic step buckling loads.

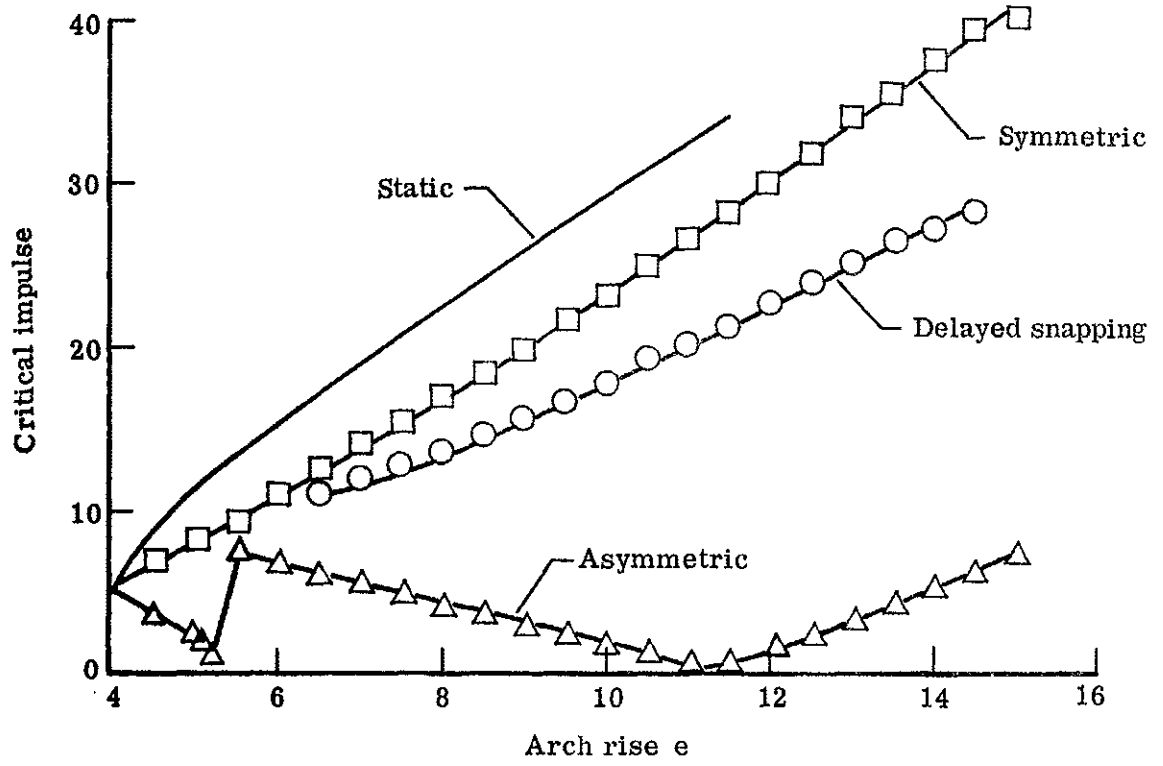


Figure 13.- Dynamic impulsive buckling loads.

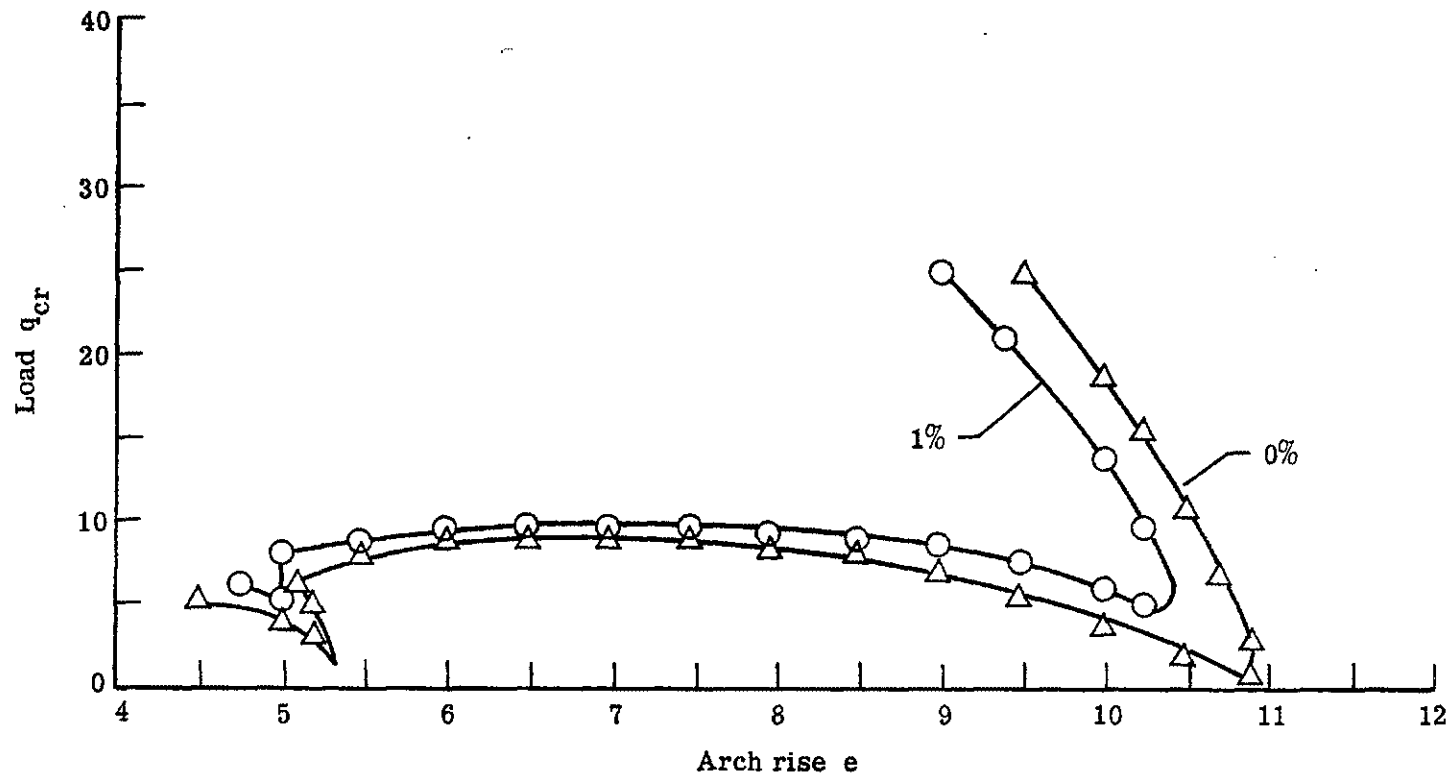


Figure 14.- Asymmetric step buckling loads with damping.

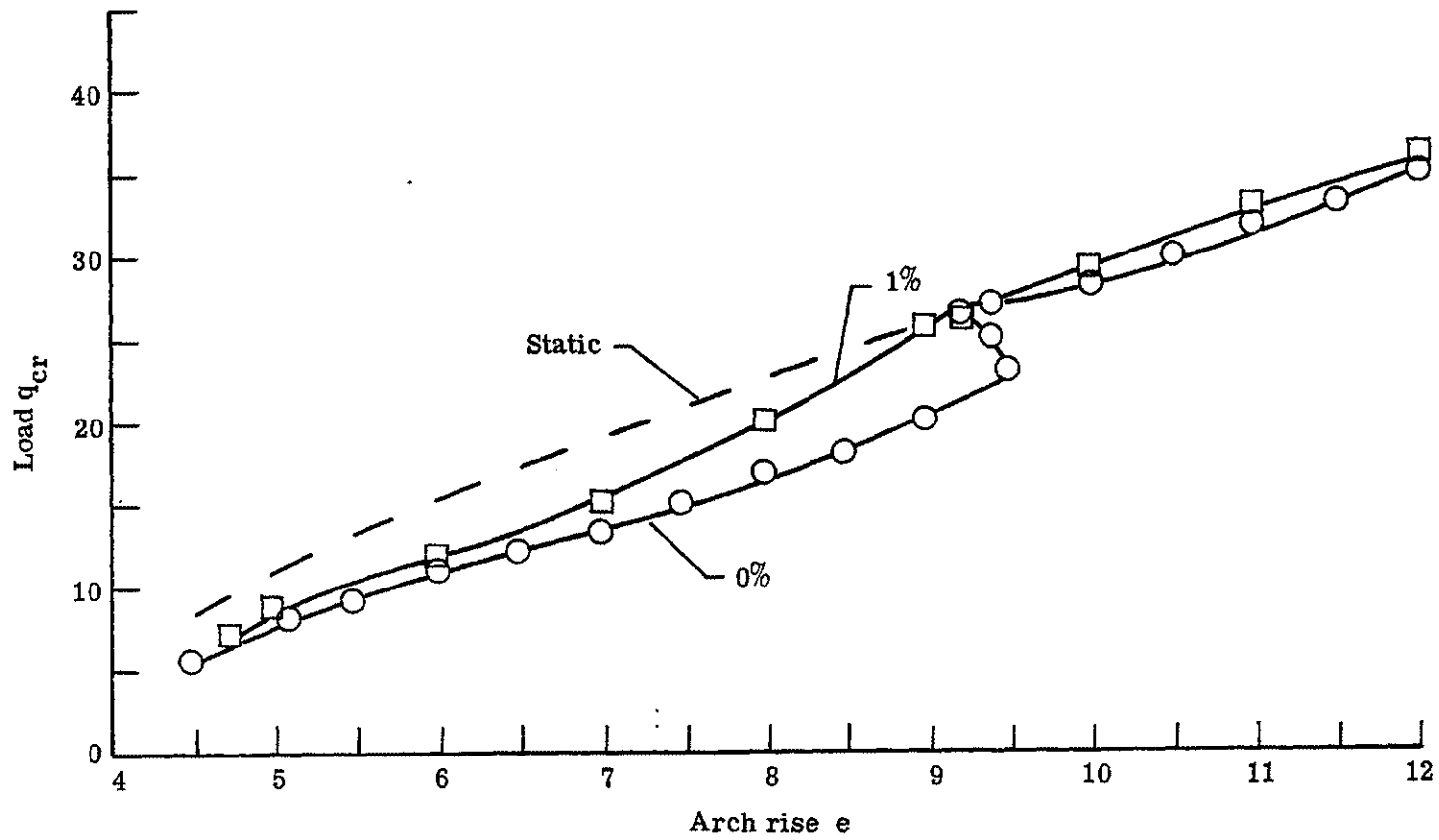


Figure 15.- Step buckling loads for delayed snapping with damping.

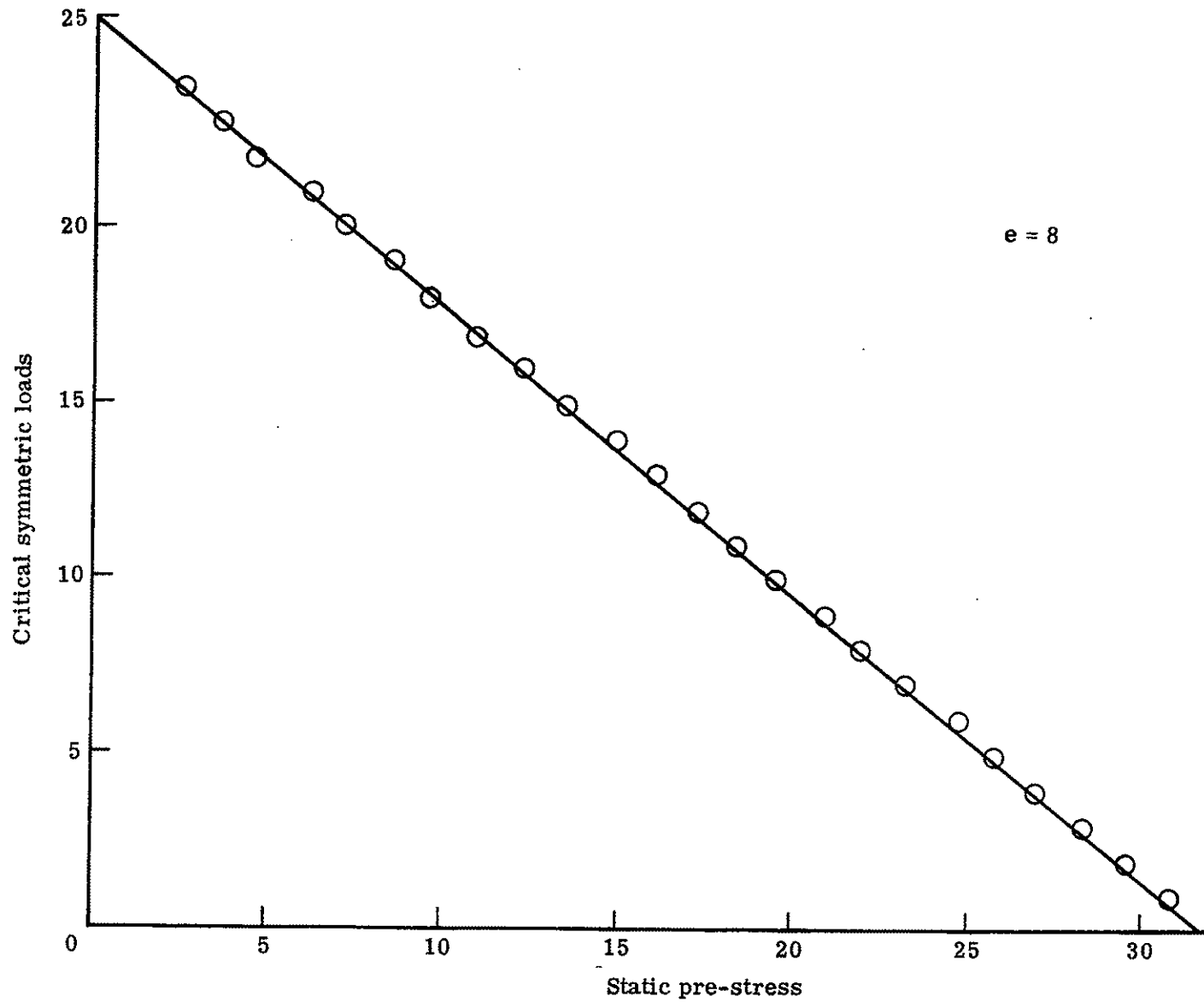


Figure 16.- Effect of static prestress on critical step symmetric loads.